2021-09-16

Fine-scale spatial and diel dynamics of zooplanktivorous fish on temperate rocky and artificial reefs

Holland, MM

10.3354/meps13831
Marine Ecology Progress Series
Inter-Research Science Center

Marine Ecology Progress Series

Manuscript:	MEPS-2021-03-047/R2 RESUBMISSION
Title:	Fine-scale spatial and diel dynamics of zooplanktivorous fish on temperate rocky and artificial reefs
Authors(s):	Matthew M Holland (Corresponding Author), Alistair Becker (Co-author), James A Smith (Co-author), Jason D Everett (Co-author), Iain M Suthers (Co-author)
Keywords:	Acoustics, Artificial reefs, Atypicthys, Echosounder, Multibeam, Planktivorous fish, Reef fish, Spatial distribution, Trachurus, WASSP, Zooplankton
Type:	Research Article

Fine-scale spatial and diel dynamics of zooplanktivorous fish on temperate rocky and artificial reefs

Matthew M. Holland[1,2,3], Alistair Becker[4], James Smith[1,5], Jason D. Everett[1,6], Iain M. Suthers[1,2]

[1] Evolution and Ecology Research Centre, School of Biological, Earth and Environmental Sciences, University of New South Wales, Sydney, NSW 2052, Australia

[2] Sydney Institute of Marine Science, Mosman, NSW 2088, Australia

[3] Marine Conservation Research Group, School of Biological and Marine Sciences, University of Plymouth, PL4 8AA, United Kingdom

[4] Port Stephens Fisheries Institute, New South Wales Department of Primary Industries, Taylors Beach, NSW 2316, Australia

[5] Institute of Marine Sciences, University of California Santa Cruz, 1156 High Street, Santa Cruz, CA 95062, USA

[6] Centre for Applications in Natural Resource Mathematics, School of Mathematics and Physics, The University of Queensland, St Lucia, QLD 4067, Australia

Target Journal: Marine Ecology Progress Series

Version 16 – 9 July 2021

Zooplanktivore spatial dynamics on temperate reefs

Abstract

Plankton is an important component of the food web in coastal reef ecosystems. Ocean currents subsidise local production by supplying plankton to resident and reef-associated planktivorous fishes. Measuring the fine-scale distribution of these schooling fishes provides insight into their habitat use and how they balance risk and reward while foraging for plankton. Maintaining their proximity to benthic structure can provide refuge from predation but may also limit foraging opportunities. We used a portable multibeam echosounder to survey schooling fish at five natural and three artificial reefs, during day and night, and under different current conditions. We isolated midwater acoustic targets and used generalised linear models to explain the distribution of schools as a function of current exposure, distance from structure and seafloor complexity. We also isolated individual schools and used generalised least squares to model how school characteristics differed between night and day, using spatial metrics of school area, perimeter length and height above the seafloor. Modelling revealed that the occurrence of schools was almost twice as likely upstream versus downstream of artificial reefs, although distance to reef structure was the main influence. School occurrence was also more likely on artificial versus natural reefs. Schools at artificial reefs exhibited greater volume and areal coverage at night, and during the day rose higher in the water column while aggregating more closely around the reef. These findings suggest that artificial and natural reefs featuring enhanced vertical relief and direct exposure to the prevailing current are preferred habitats for planktivorous fish.

Keywords: artificial reefs, *Atypicthys*, echosounder, multibeam, reef fish, spatial distribution, *Trachurus*, WASSP, zooplanktivores

1. Introduction

Reef ecosystems are supported by a combination of benthic productivity and pelagic subsidies from plankton (Morais & Bellwood 2019, Puckeridge et al. 2021, Skinner et al. 2021). Planktonic production often contributes more energy than benthic production because it is generated over a larger area and delivered to the reef by ocean currents (Docmac et al. 2017, Udy et al. 2019, Zuercher & Galloway 2019, Skinner et al. 2021). This supply of plankton is influenced by multiple processes including current speed and direction, upwelling, productivity, and upstream consumption. Plankton can support over half of reef-associated fish biomass (Truong et al. 2017, Holland et al. 2020), especially when reefs exist as pockets of structural complexity in otherwise relatively featureless sandy environments (Morais & Bellwood 2019, Zuercher & Galloway 2019).

Due to their high abundance and frequency as prey, planktivorous fish are a key pathway by which planktonic energy supports reef food webs (Bakun 2006, Pikitch et al. 2014). To reduce their individual risk of predation, these fish form schools or aggregations and often maintain their proximity to the reef structure while feeding on zooplankton (Motro et al. 2005, Yahel et al. 2005b, Champion et al. 2015, Paxton et al. 2019). Proximity to structure provides access to physical refuges where fish can shelter to escape or avoid predators (Borland et al. 2021). An indirect benefit of aggregation behaviour results when schools associate with the same object (Sandin & Pacala 2005), providing increased vigilance, confusing predators, and diluting individual predation risk (Morgan & Godin 1985). Individual fish must also compete with their neighbours for access to this dispersed food source and there may be a benefit to spreading out and reducing their density, with the trade-off of increased distance to reef structure and consequently increased predation risk (Motro et al., 2005).

As current driven zooplankton are encountered by reef-associated planktivorous fish, they are grazed upon as they pass over the reef. This process, referred to as the 'Wall of Mouths' (Hamner et al. 1988), can deplete zooplankton density across tropical coral reefs (Kiflawi & Genin 1997, Holzman et al. 2005, Motro et al. 2005, Yahel et al. 2005b) by up to 45% h^{-1} (Gal 1993). Tropical coral reefs tend to exhibit a common morphology, making such gradients in zooplankton density possible because currents bearing pelagic zooplankton must first pass from the open ocean over the reef crest before reaching the reef flat. Temperate rocky reefs can exhibit very different morphology, with no analogous barrier or bottleneck, making large-scale gradients in zooplankton density unlikely. While such large-scale zooplankton depletion may be challenging to observe along temperate rocky reef coastlines, localised depletion of zooplankton density has been observed across individual temperate rocky reefs (Kingsford & MacDiarmid 1988, Paxton et al. 2019).

As zooplanktivore feeding rates can be highly correlated with zooplankton density (Kiflawi & Genin 1997), localised depletion may be an important process structuring the small-scale distribution of schools. An obvious solution to improve individual foraging success within a school is to disperse, both vertically and horizontally. The limited vertical relief of many temperate rocky reefs requires fish to feed higher in the water column, thus increasing distance from the safety afforded by physical structure (Motro et al. 2005). Similarly, in the case of isolated reefs such as patch reefs and artificial structures, spreading out horizontally also increases distance from reef structure.

Designed artificial reefs are increasingly being deployed for fisheries enhancement and habitat restoration, incorporating features intended to improve recruitment and sustain large schools of associated zooplanktivores (Sherman et al. 2002). Effective designs typically incorporate multiple structures arranged across a wide horizontal footprint (Becker et al.

2019), with the structures themselves containing internal spaces (Sherman et al. 2002), and exaggerated vertical relief (Rilov & Benayahu 2002, Davis & Smith 2017). Vertical relief may facilitate attraction and recruitment by encouraging the settlement of near-surface fish larvae as they move inshore, or by allowing fish to feed in a section of the water column with greater flux of zooplankton (Rilov & Benayahu 2002). Artificial reefs normally contain tall vertical features and are consistently found to support greater fish abundance than natural reef habitats (Rilov & Benayahu 2000, Claisse et al. 2014). However, only a few studies have examined how schooling fish use this enhanced vertical relief (Sala et al. 2007, Champion et al. 2015, Becker et al. 2019, Borland et al. 2021).

The goal of this study was to evaluate schooling behaviour of planktivorous fish using multibeam echosounders (MBES) in rocky reef ecosystems. We used artificial reefs as model systems to document how fish school around isolated high vertical relief structures and compared these to nearby natural reefs to determine whether aggregation behaviours measured at artificial reefs could also be observed across less abrupt natural topography. Our specific aims were to: (1) examine school distribution relative to fine-scale variation in benthic structure and current direction; (2) quantify differences in the distribution and composition of schooling fish at an artificial and a natural reef and between night and day; and (3) quantify the zooplankton supply to temperate reefs. The results of this study reveal the behaviours of planktivorous fish which enable the important trophic link between plankton and predators and allow us to better understand how they use artificial habitats.

2. Methods

2.1. Site selection

Fieldwork was conducted off the coast from Sydney, Australia (33.87° S, 151.21° E), where up to 71% of fish biomass around rocky reefs consists of schooling zooplanktivores (Truong

et al. 2017). In total, eight sites were selected (Figure 1). These consisted of a northern group and a southern group which were surveyed separately. The sites consisted of five natural reef locations, a heavily eroded shipwreck ('Annie Miller', AM), and two designed artificial reefs. The two designed artificial reefs were deployed to improve fishing opportunities for recreational anglers, with one constructed from steel (Offshore Artificial Reef, OAR, Scott et al. 2015) and the other consisting of a 'reef field' of concrete modules (John Dunphy Reef, JDN, Becker et al. 2019). Both designed artificial reefs had towers to enhance their vertical relief to 8 to 12 m.

Of the eight sites, the northern six (four natural, two artificial) were selected to examine school distribution relative to fine-scale variation in benthic structure and current direction (Aim 1; Table 1). The remaining two southern sites (one natural, one artificial) were selected to quantify differences in the distribution and composition of schooling fish at night and during day, and to measure zooplankton supply (Aims 2, 3; Table 1). These two relatively isolated sites were selected for safety reasons due to the requirements of working at night. These two sites were located further south than the other six and thus it was impractical to include them in the other survey.

2.2. Data collection

2.2.1. School distribution

School distribution surveys (six sites; Table 1) were conducted from a 6.5 metre vessel. A WASSP WMB-1320Fi portable 160 kHz multi-beam echosounder (WASSP Limited, Auckland, New Zealand) was used to record tide-corrected bathymetry and water column targets simultaneously. The transducer was mounted over the gunwale with an integrated Hemisphere Vector V103 Smart Antenna (Hemisphere GNSS, Scottsdale, United States),

adjusting for pitch, heave and roll in real-time. For each survey, seven parallel 200 m transects were conducted at ~2.5 m s^{-1}, initially aligned into the prevailing swell (Figure S1a).

To characterise current velocity and bearing, a remote camera drifter was deployed during each survey. This consisted of a float attached to 20 m of rope with a steel frame to act as a drogue, supporting two opposite-facing GoPro Hero 4 cameras (GoPro Inc., San Mateo, United States), as in Smith et al. (2017), to record fish species present (Figure S2). The cameras were included as a means of ground-truthing the likely fish species detected on the echosounder as species identification based on acoustic data alone is difficult. The rope length (20 m) was chosen as a compromise to ensure the camera assembly did not touch the seafloor at any of the sites. While it was certainly possible for this drifter to be affected by wind or vertically sheared currents (Lumpkin et al. 2017), surveys were conducted on days with negligible wind to improve the quality of acoustic data, so any deviance from true current bearing was expected to be minor. Due to the modest size of the drogue, it is likely that total drift did not equal current flow, although it was likely to be proportional.

Footage was observed in its entirety and species observations were recorded. Since many video deployments did not observe fish, despite schools being detected by the echosounder in all surveys, footage was only suitable for determining species presence. The drift of the camera assembly was used to calculate current velocity and bearing.

2.2.2. Diel effects on school characteristics and zooplankton supply

School characteristics surveys (two sites; Table 1) were conducted from a 14 m wooden vessel. The same MBES was used to record bathymetry and water column targets, at ~2.5 m s^{-1}. To ensure a similar area of seafloor was surveyed at each of the two sites, five parallel 300 m transects (along lines of constant longitude) were conducted at the artificial reef (Figure S1b), while nine transects were conducted at the shallower natural reef (Figure 1).

Each site was surveyed before and after sunrise, with a one-hour buffer either side of sunrise to avoid the morning crepuscular period (Yahel et al. 2005a, Myers et al. 2016) and subsequent surveys of the same reef were separated by over four hours.

Since our uncalibrated MBES was incapable of measuring zooplankton biomass using approaches such as dB differencing (Colbo et al. 2014) we sampled midwater zooplankton in situ. Following each acoustic survey two replicate horizontal tows were conducted using a 40 cm diameter circular net with a 200 μm mesh for 5 minutes per tow. Through visually monitoring the angle of the tow rope a vessel speed of ~1.25 m s^{-1} was selected in order to effectively sample the water column at ~15 m depth, while also capturing zooplankton at the surface incidentally as the net was deployed and retrieved. This tow depth provided a 5 m gap above the top of the natural reef and the artificial reef towers to avoid damage to the net. Thus, zooplankton density we measured may differ from zooplankton density closer to the reef structures or the seafloor. A mechanical flowmeter (General Oceanics, Miami, USA) was used to calculate volume of water filtered. Samples were preserved in a 5% formaldehyde solution for laboratory post-processing.

After each post-sunrise survey, the same remote camera assembly was deployed for 30 minutes at the centre of each reef to identify the fish species assemblage. It was fitted with an anchor to suspend cameras ~2.5 m above the seafloor, similar to Sheehan et al. (2020), to improve the chance of recording schools. Instead of using a drifter, current velocity and bearing were determined based on drift of the vessel's GPS position while engines were in neutral. The effect of wind was considered minimal, as the 40-tonne vessel had a 3 m deep keel, and all surveys took place on days with negligible wind to improve data quality. Since residual surface currents are primarily propagated by wind, with a magnitude of ~1-2% of

wind speed (Prandle & Matthews 1990), it is likely that vessel drift was primarily driven by bulk current flow.

2.3. Data processing

2.3.1. Water column acoustic data

For both studies, raw acoustic data were initially processed using Echoview v10.0 (Echoview Software Pty Ltd, Hobart, Australia) to isolate fish targets from noise and bottom backscatter (Holland et al. 2021). We applied image filtering methods (e.g. convolution, erosion) from Holland et al. (2021) to generated a three-dimensional Boolean mask to define spatial envelopes to represent school boundaries and extract the raw MBES data.

Since it is often difficult to differentiate between reef structure and demersal fish acoustically, bathymetry surfaces generated from a previous LiDAR survey were used to mask out data below the seafloor (NSW Department of Planning Industry and Environment 2018). Even still, it is likely that some fish near the seafloor were obscured by natural and artificial structures.

Georeferenced samples were then exported from Echoview and all further analysis was conducted in R v3.6.3 (R Core Team 2020). We projected the extracted data over a grid and measured the water column depth of the highest and lowest fish target occurring over each grid cell to delineate the gridded horizontal distribution of school thickness (explained in detail in Supplementary, Text S1). Like many MBES, the WASSP cannot be used to quantify fish abundance based on backscattering data; we therefore used variation in school thickness as a proxy to examine school distribution (Figure 2; Holland et al. 2021).

Variability among surveys and transects in the fish abundance contained within measured levels of school thickness is inevitable. School thickness in this case is likely a poor index of

absolute fish abundance, and is best interpreted as a depth-aggregated proxy of relative fish abundance (Misund et al. 1995, Holland et al. 2021). This is an appropriate metric as our study was concerned with the spatial distribution of schools relative to the current, to structure, and to a changing bathymetry.

2.3.2. School distribution

For the study of school distribution (Aim 1; Table 1), raw point clouds generated by the WASSP software's bathymetry detection algorithm were projected and rasterised over a 200 m square grid with 5 m resolution. The 'terrain' function in the 'raster' package (Hijmans 2020) was used to calculate seafloor aspect and roughness for natural reef sites (Wilson et al. 2007). Roughness was calculated as the difference between the minimum and maximum depths of each cell and an unweighted kernel of its eight neighbouring cells (Borland et al. 2021). This measurement assigns greater values to seafloor with steep slope and high complexity (Wilson et al. 2007).

To represent the degree of exposure to prevailing currents for artificial reef sites, a continuous raster surface was generated, where cells directly upstream of the reef were assigned a value of 1 and cells directly downstream of the reef, a value of 0 (Figure S3a). We refer to this indicator variable hereafter as 'relative bearing'. Similarly, for natural reef sites we calculated 'relative aspect' by assigning seafloor aspects directly facing the prevailing current a value of 1, and aspects facing away from the current, a value of 0 (Figure S3b). Remaining bearings were interpolated between these two values.

These 'relative bearing' and 'relative aspect' variables were calculated for each survey to account for variation in current direction. These two variables were used to measure upstream versus downstream preference. It was necessary to apply separate indicator variables for natural versus artificial reefs due to there being no clearly defined boundaries or single point

of high vertical relief around which to measure current exposure across continuous habitat at natural reefs.

2.3.3. Diel effects on school characteristics

For the study of school characteristics, all rasterised transects were processed individually using image analysis techniques and kernel functions to isolate individual aggregations or schools, following methods from Reid and Simmonds (1993), which outlined image analysis techniques for isolating fish schools from vertical acoustic profiles (Figure S4, explained in Supplementary, Text S2).

2.4. Data analysis

While most of our analysis focused on investigating differences between natural and artificial reefs, it is important to note that differences in the physical variables we measured (diel behaviour, position in the water column, etc.) may be attributable to fundamental differences between natural and artificial reefs, or they may be due to differences in species assemblages. In this case differences between reef types cover both possibilities and the data at hand does not allow these two alternatives to be resolved.

2.4.1. Modelling school distribution

Gridded school thickness, derived from the water column acoustic data (Holland et al. 2021), was indexed with gridded environmental variables to model school thickness relative to seafloor characteristics. Artificial reefs were modelled separately to natural reefs. There were naturally many grid cells in a typical survey which did not contain fish, thus data were highly zero-inflated. Because of the zero-inflation of school thickness, and its uncertain association with fish abundance, we modelled the binomial probability (0 to 1) of fish school presence at reef sites using generalised linear models (GLMs).

The artificial reefs GLM included the following explanatory variables: 'distance from reef', 'relative bearing', 'reef site' as a fixed effect (n = 2) to account for a difference in school occurrence between the two artificial reefs, and 'date' as a fixed effect (n = 4) to account for variation in environmental condition amongst surveys, as described below (in script notation):

$$\text{glm}(\text{Presence} \sim \text{reef site} + \text{date} + \text{distance from reef} + \text{relative bearing}, \text{family} = \text{binomial}(\text{link} = \text{logit})) \quad (1)$$

We compared this full model with a restricted 'reef site only' model, using the Akaike Information Criterion (AIC), to evaluate the contribution of the spatial variables to explained information. We calculated area under the curve (AUC) of the full model to evaluate goodness-of-fit (Elith et al. 2006) and generated a one-dimensional prediction to examine the combined effects of the two covariates (distance and relative bearing) on probability of school occurrence. Finally, we generated a semivariogram from Pearson residuals to visually assess spatial autocorrelation. This model satisfied all assumptions regarding the normal distribution of residuals and quantile-quantile plots. The semivariogram generated from the final model (Figure S5a) suggested no change in semivariance with increases in spatial separation, and thus no residual spatial autocorrelation.

The natural reef GLM was similar to the artificial reef GLM, but as previously mentioned because natural reefs do not contain an appropriate location from which to measure 'distance from reef', we included the explanatory variables 'roughness' and 'relative aspect'. In this case, 'roughness' was used to represent variation in bathymetry and 'relative aspect' was used to represent current exposure. This model was subject to the same validation process as the artificial reef GLM, and similarly indicated no evidence of spatial autocorrelation (Figure S5b). Model structure is described below (in script notation):

$$\text{glm}(\text{Presence} \sim \text{reef site} + \text{date} + \text{roughness} + \text{relative aspect}, \text{family} = \text{binomial}(\text{link} = \text{logit})) \quad (2)$$

2.4.2. Modelling diel effects on school characteristics

We used the extracted fish aggregations to examine differences in school size and number of schools between sites and between night and day. We calculated schools per unit area, and the mean area and volume contained within a school, inclusive of empty space unoccupied by fish within each school boundary resolved by the image analysis process. Mean school size and school abundance values (per transect) were used as responses in three generalised least squares (GLS) models, with the following structure (in script notation):

$$\text{gls}(\text{Response} \sim \text{diel} * \text{reef} + \text{date}, \text{correlation} = \text{corGaus}(\text{formula} = \sim \text{mean\_x} + \text{mean\_y} \mid \text{survey}), \text{method} = \text{'ML'}) \quad (3)$$

Where 'Response' is 'schools per unit area', 'area per school' or 'volume per school', 'diel' is a factor with two levels for diel period (night or day), 'reef' is a factor with two levels (N5 or JDN), 'date' is an unordered factor to account for day-to-day variability (7 levels) consistent across diel period and sites. This model structure was selected to test whether diel differences were consistent across reef sites, while allowing for mean differences in the response variable among surveys. A Gaussian correlation structure was included to account for possible spatial autocorrelation of residual values. Correlation structure inputs ('mean_x' and 'mean_y') were calculated as the centroid coordinates for each transect. Residuals were assessed for normality and fitted models were compared to identical models with 'date' as the only predictor (lacking the interaction term 'diel * reef') using the likelihood-ratio test and through examining ΔAIC. A caveat of this approach is that when school width exceeds the swath width, the average area of the school is underestimated; thus, any patterns in the

distribution of very large schools (that exceed swath width) are not properly estimated as schools can only be as large as the swath itself.

To examine diel differences in vertical distribution, extracted fish aggregations were used to calculate mean per transect values for ‘school thickness’ and ‘height above bottom’. Height above bottom was calculated as the difference between seafloor depth and the deepest target (Weber et al. 2009). GLS models were fit for each of these two response variables, with identical structure and validation as in the previous example (Equation 3).

Extracted fish aggregations were used to calculate the ‘perimeter to area’ and the ‘area to volume’ ratios for each distinct school. Whereas area and volume indicate school size, these metrics indicate school diffuseness. Mean per transect values were used as response variables in two GLS models (Equation 3). In cases where schools exceeded swath width, swath sides were considered part of the school perimeter.

Similarly, we examined the horizontal position of schools relative to the centre of each reef, by calculating the distance from each school centroid to the reef centre. For the artificial reef, we considered the reef centre to be the centroid of concrete modules, and for the natural reef we used the peak of bathymetry. We generated a GLS model with identical structure to the previous examples (Equation 3), but with correlation structure represented by school centroid coordinates.

2.4.3. Underwater video analysis

Video was analysed by subsampling each thirty-minute deployment as five randomly selected two-minute intervals, as in Basford et al. (2016). To minimise temporal autocorrelation each sample had a gap of at least two minutes from adjacent samples. We recorded the maximum number of individuals of a species observable within a single frame (MaxN) (Campbell et al.

2015). When large schools were observed, fish were counted from screenshots using the 'multi-point' counting tool in ImageJ (National Institute of Health, Washington D.C., USA). The maximum abundance of each species observed across both opposite-facing cameras was recorded as MaxN for each time interval (Becker et al. 2019).

A relative abundance matrix was generated for the five schooling species observed during the study. Non-schooling species and species recorded only once (e.g. blue-spotted flathead (*Platycephalus caeruleopunctatus*), red morwong (*Cheilodactylus fuscus*), Port Jackson shark (*Heterodontus portusjacksoni*)) were excluded from analysis. We conducted a multivariate analysis to examine differences in fish community between the natural and artificial reefs. Further univariate analysis was conducted to resolve drivers of differences and similarities.

For the multivariate analysis, we generated a generalised linear latent variable model (GLLVM) using the R package 'gllvm' (Niku et al. 2020). We modelled count data, including an observation-level (i.e. row) factor to control for differences in abundance among surveys, using the following formula (in script notation):

$$\begin{aligned}\mathrm{gllvm}(y = \mathrm{Abundance}, X = \mathrm{environmental\_variables}, \mathrm{num.lv} = 2, \mathrm{family} \\ = \mathrm{poisson}, \mathrm{row.eff} = \mathrm{TRUE}, \mathrm{formula} = \sim \mathrm{date} + \mathrm{reef})\end{aligned} \quad (4)$$

Where 'Abundance' is the matrix of species relative abundances (n = 70 observations), 'environmental_variables' is a matrix of environmental variables, modelled as a function of two latent variables and factors for 'date' and 'reef'. The variable 'reef' was included as a factor with two levels. Ordination plots were generated from this model but with the 'reef' term removed and covariate coefficient plots were generated with the 'date' term removed to visualise general patterns in two dimensions.

For further univariate analysis we calculated total fish abundance (by taking the sum of MaxNs for each species observed within a sample), species richness and the Shannon diversity index for each video sample. These three variables were used as the response for three GLS models with the following structure (in script notation):

$$\text{gls}(\text{Response} \sim \text{reef} + \text{date}, \text{correlation} = \text{corCAR1}(\text{form} = \sim\text{time} \mid \text{survey}), \text{method} = \text{'ML'}) \quad (5)$$

Where 'Response' (n = 70 observations) is the abundance, species richness or Shannon diversity index of samples. We defined a continuous AR1 correlation structure (corCAR1), with 'time' as the video time stamp and 'survey' as a grouping factor for each video deployment (i.e. to group each set of five sub-samples).

For validation, each multivariate and univariate model was assessed for normality of residuals and was compared to a nested model with 'date' as the only predictor (excluding the 'reef' term) using the likelihood-ratio test and through examining ΔAIC.

2.4.4. Zooplankton density and flux

To quantify zooplankton biomass and abundance, zooplankton samples were processed through a lab-based Laser Optical Particle Counter (LOPC) (Rolls Royce Canada Ltd, Peterborough, Canada) connected to a flow through system (Moore & Suthers 2006). Zooplankton samples were subsampled 1/2 to 1/8 of their original volume, depending on sample density. Post-processing of the binary LOPC output was performed using MATLAB (MathWorks, Natick, United States). Equivalent spherical diameter (ESD) of measured particles (346 to 30,000 μm ESD) was used to calculate volume contained within each particle, assuming ESD to be the longest dimension of an oblate ellipsoid with a 3:1 ratio. Volumes were converted to biomass density (mg m^{-3}) using the density of water and the volume of water filtered (Suthers et al. 2006).

To confirm whether zooplankton samples were representative of the prey resident zooplanktivores were feeding on and to alleviate concerns regarding net avoidance, we compared the size distribution of net samples with size distribution obtained from a local diet analysis (Schilling et al. unpublished data). Average size distributions for day and night zooplankton samples were generated to be compared to similar size distributions obtained from the gut contents analysis for three of the most abundant species of zooplanktivore in the region.

To measure the rate of zooplankton delivery to the artificial reef (JDN), we calculated the mean current bearing across all surveys and estimated the area of the reef field profile (i.e. the vertical area) perpendicular to this bearing, using 95% confidence intervals for the mean height above bottom of fish targets as the vertical dimension. We calculated the rate of zooplankton delivery (in g s^{-1}), by multiplying the biomass density (g m^{-3}) by the current velocity (m s^{-1}) to derive zooplankton flux (g m^{-2} s^{-1}) and multiplying by the reef profile area (m^2). We did not calculate zooplankton delivery for the natural reef, as the site had less well-defined boundaries. We interpreted differences in zooplankton abundance and biomass (from lab-processed zooplankton samples) as evidence of localised depletion by zooplanktivores. While additional zooplankton sampling in the absence of fish may have been useful in identifying whether night versus day differences were a direct result of depletion by fish, this was not possible due to the timing constraints of pre-dawn surveys.

3. Results

3.1. School composition and diversity

Two schooling fish species (*Trachurus novaezelandiae* and *Pseudocaranx georgianus*) were observed from the drift camera assembly at artificial reefs. These fish were only observed during one survey. At the natural reefs, six species were observed (*Trachurus*

novaezelandiae, Pseudocaranx georgianus, Chromis hypsilepis, Scorpis lineolata, Atypicthys strigatus and *Seriola lalandi*). The drifting midwater cameras had low success in observing fish, despite schools being detected by the MBES during all surveys.

Greater success was achieved using the stationary benthic camera when evaluating school characteristics. Five schooling species were detected (*Trachurus novaezelandiae, Pseudocaranx georgianus, Chromis hypsilepis, Scorpis lineolata* and *Atypicthys strigatus*). All species except *P. georgianus* were zooplanktivores (Froese & Pauly 2009). The covariate coefficient plot indicates that *T. novaezelandiae* was just as likely to be found at either reef, whereas all other taxa were more likely to be found at N5 (Figure 3).

The GLLVM was found to outperform the null model when the fixed term for 'reef site' was included as a predictor ($\Delta AIC = 78.1$, $p < 0.001$), indicating that the artificial and natural reef sites contained statistically distinct fish community composition. The ordination indicates this difference in composition, especially along the LV2 axis (Figure 4). Clustering of survey date indicates structure at the weekly-monthly scale. Coefficient plots and confidence intervals for each species plotted against reef site indicate differences were driven by highly abundant *T. novaezelandiae* at the artificial reef, and by *S. lineolata, C. hypsilepis* and *P. georgianus* at the natural reef. *A. strigatus* was just as likely to be found at either site.

The artificial reef hosted greater total abundance than the natural reef (Figure 5a) (coeff. = 82.8, $p = 0.013$) (Table S1), however, it also hosted lower species richness (Figure 5b) (coeff. = -1.17, $p < 0.001$) and Shannon diversity (Figure 5c) (coeff. = -0.32, $p < 0.001$).

3.2. School distribution at artificial reefs

For the GLM modelling school presence at the artificial reef, the full model had a much lower AIC than a model including only site ($\Delta AIC = 4727$), indicating distance and bearing

to reef were important (Table 2). Effects plots indicate a slightly greater probability of schools occurring in any cell (Figure 6a) at the AM reef versus the OAR (Table 2; $p < 0.001$). Schools were much more frequently detected during the 2018-11-19 survey (Figure 6b), reflecting the patterns observed in Figure 2. Probability of school occurrence declined with increasing distance from the reef (Figure 6c). Although there was a preference for upstream orientation, with schools almost twice as likely upstream versus downstream (Figure 6d), it was predominantly distance to reef affecting school occurrence. The prediction for fish school presence around a simulated artificial reef (Figure 7) highlights that schools were generally centred over the reef structure, with slight preference for the upstream side of the reef.

3.3. School distribution at natural reefs

For the GLM modelling school presence at the natural reefs (Table 2), AIC increased with removal of the roughness term (ΔAIC = -344) and with removal of the relative aspect term (ΔAIC = -9.3), suggesting all model terms were important. Effects plots indicated variable probability of school occurrence among reef sites (Figure 6e), with the greatest probability at N1 and the least, N3. Schools were most frequently detected during the 2018-12-05 survey (Figure 6f). Probability of school occurrence was positively correlated with seafloor roughness (Figure 6g). Upstream aspects had a slightly greater probability of school occurrence (Figure 6h); however, the magnitude of this effect was less important than the effect of roughness, and less strong than observed on artificial reefs.

3.4. Diel effects on school characteristics

Fish school attributes measured with the MBES were examined using GLS models to test for differences in spatial characteristics between sites and between night and day (Table S2). The GLS model for mean area covered by a contiguous school (m^2) (Figure 8a) indicated a

significant interaction of diel period and reef site, such that schools at the artificial reef were smaller during day (coeff. = -1603.2, $p < 0.001$). There was a significant interaction of diel period and reef site (Figure 8b), such that the proportion of area covered by schools decreased between night and day at the artificial reef only (coeff. = -0.15, $p < 0.001$). Mean school volume (m^3) (Figure 8c) did not differ between night and day (coeff. = 789, $p = 0.665$), however schools at the artificial reef had greater overall volume (coeff. = 12627, $p < 0.001$). Across both sites there were fewer individual schools during the day (coeff. = -5.56, $p < 0.001$) (Figure 8d).

Mean school height above bottom (m) was greater during the day (coeff. = 0.75, $p = 0.012$) and at the artificial reef (coeff. = 1.16, $p = 0.001$)(Figure 8e). Mean school thickness (m) was also significantly greater during the day (coeff. = 1.50, $p < 0.001$) and at the artificial reef (coeff. = 2.18, $p < 0.001$)(Figure 8f).

The mean perimeter to area ratio (Figure 8g) was lower during the day (coeff. = -0.18, $p = 0.008$), indicating that schools were more diffuse at night. Perimeter to area ratio at the artificial reef was lower than at the natural reef (coeff. = -0.30, $p < 0.001$). The area to volume ratio (Figure 8h) indicated that schools had a more compact three-dimensional structure during the day (coeff. = -0.08, $p < 0.001$) and schools were also more compact at the artificial reef site (coeff. = -0.09, $p < 0.001$). Schools at the artificial reef were located closer to the centre of the reef during the day (Figure 8i), as indicated by a significant interaction effect of reef site and diel period (coeff. = -13.2, $p = 0.024$).

3.5. Current and zooplankton density

The size distributions of zooplankton samples showed strong overlap with the size distributions of prey obtained from gut contents analysis (Figure S6). Our zooplankton net samples collected a greater proportion of zooplankton in the larger size bins than was present

in the gut contents of three of the most abundant zooplanktivores species (Schilling et al. unpublished data), suggesting that we adequately captured the range of zooplankters being captured as prey.

There was no difference in zooplankton abundance between night and day during our sampling period (± SE) at either N5 (coeff. = 342, p = 0.79) or JDN (coeff. = 659, p = 0.68) (N5: night = 3745 ± 916, day = 4087 ± 765, JDN: night = 4510 ± 1582, day = 5169 ± 1004 ind. m^{-3}). No significant difference was found in zooplankton biomass between night and day (± SE) at either N5 (coeff. = 16, p = 0.89) or JDN (coeff. = 231, p = 0.37) (N5: night = 317 ± 56, day = 333 ± 57, JDN: night = 396 ± 121, day = 628 ± 130 mg m^{-3}). While this lack of difference is surprising considering the universality of diel vertical migration, it may be attributable to the relatively low sample size and natural patchiness of zooplankton distribution.

Based on mean current velocity and bearing (± SE) (0.33 ± 0.02 m s^{-1} at 173 ± 10°), and mean biomass density recorded at JDN (day: 628 ± 130, night: 396 ± 212 mg m^{-3}), we calculated the horizontal flux of zooplankton as: day = 207 ± 43, and night = 131 ± 40 mg m^{-2} s^{-1}. Based on a rectangular cross-section of the reef profile, calculated using the width of the reef in the dimension perpendicular to the current (136 m) and height above bottom for 95% of samples (day: 4.2 m, night: 3.4 m), net zooplankton delivery to JDN was 118 ± 25 g s^{-1} during the day (or 425 ± 90 kg h^{-1}) and 61 ± 18 g s^{-1} at night (or 220 ± 65 kg h^{-1}). Divided evenly across the reef area (9800 m^2), this was 43 ± 9 g m^{-2} h^{-1} during day and 22 ± 7 g m^{-2} h^{-1} at night. We estimate that zooplankton supply to JDN, based on the length of the reef cross-section aligned with current (143 m) and current velocity of 0.33 m s^{-1}, would turnover completely every 7 minutes.

4. Discussion

This study reveals dynamic patterns in the behaviour of schooling zooplanktivores at artificial and natural rocky reefs. Through measuring variation in the distribution and spatial characteristics of schools we have gained insight into the behaviour of reef-associated schooling fish. Across natural and artificial habitats, schools demonstrated an affinity for vertical relief and a preference for the upstream side of benthic structure. This upstream preference suggests fish distribution may be influenced by intra-school prey depletion (Paxton et al. 2019), as fish compete for preferential access to prey delivered by the current.

Artificial reefs were also more likely than natural reefs to host large schools of zooplanktivores, exhibiting greater volume and areal coverage at night and rising higher in the water column while aggregating closer around the reef during the day. The novel physical structure provided by the artificial reef may have facilitated differences in how schooling fish utilised space within their environment and supported a fish community distinct from that of the nearby natural reef (Becker et al. 2017).

4.1. Zooplanktivores and the prey that sustains them

The video surveys used to ground-truth the species detected by the MBES revealed that two species dominated the patterns in our study, *Trachurus novaezelandiae* and *Atypicthys strigatus*, and were the only species observed in high abundance. Both species feed almost exclusively on zooplanktivores throughout their lives (Champion et al. 2015, Dawson et al. 2020). As *A. strigatus* was less abundant than *T. novaezelandiae*, and because *A. strigatus* generally maintains close proximity to reef structure (Champion et al. 2015), it is likely the broad patterns we observed across the artificial reef field were driven primarily by *T. novaezelandiae*. This is consistent with other studies of community composition on artificial reefs in the same region (Scott et al. 2015, Smith et al. 2017).

The large zooplankton flux we measured, and the rate at which it was replenished across the artificial reef field by the prevailing current, suggests that fish are unlikely to be limited by overall prey availability. While we acknowledge that localised depletion of zooplankton by fish could have impacted our calculations of zooplankton delivery rates, the values we recorded were still very high. It is generally accepted that temperate reefs receive more than adequate delivery of zooplankton to achieve maximum growth rates in planktivorous reef fishes, however, this is not always the case (Anderson & Sabado 1995). The 43 g m^{-2} h^{-1} zooplankton flux we measured should be adequate to sustain a large population of zooplanktivores, considering that an adult (34 g) *A. strigatus* consumes only 0.77 g day^{-1} (Champion et al. 2015) and an adult (100 g) *T. novaezelandiae* consumes 1.85 g day^{-1} (Dawson et al. 2020). If these fish can only visually forage for 12 hours per day, each square metre of reef could potentially support up to 670 individual (or 23 kg) *A. strigatus* or 279 individual (or 27.9 kg) *T. novaezelandiae*, assuming all zooplankton passing through the reef are consumed, and that prey density across the reef is uniform. While these assumptions are unlikely (Kiflawi & Genin 1997), they provide evidence that fish assemblages on coastal reefs in this region are unlikely to be limited by zooplankton.

4.2. Foraging behaviour may drive spatial distribution around structure

Even with such a large abundance of zooplankton, there was evidence that intra-school foraging competition may have helped structure school distribution around natural and artificial reefs. We observed similarities across the two habitat types in the distribution of schools relative to variation in benthic structure and current direction. Fish demonstrated a preference for orienting towards the upstream side, possibly to gain ‘first’ access to zooplankton, before it could be accessed by other reef organisms.

This tendency to forage upstream of structure has been observed across several studies (Hobson & Chess 1978, Bray 1980, Kingsford & MacDiarmid 1988, Forrester 1991, Paxton et al. 2019). As zooplankton are delivered by current, fish have a limited window or 'reactive volume' within which to notice and react to drifting prey items (Kiflawi & Genin 1997). Fish positioned back from the leading edge of a school have a reduced reactive volume, as their field of vision is obstructed by fish upstream (O'Brien 1979). They also experience reduced prey density, as upstream fish pick off the larger, more visually apparent and thus likely more nutritious prey items (Forrester 1991). Diver-based studies have documented these localised reductions in zooplankton density co-occurring with gradients in predation pressure (Kingsford & MacDiarmid 1988, Motro et al. 2005). Fish that position themselves at the leading edge of schools may stand to improve their feeding rate. Thus, while the biomass of zooplankton delivered to large reefs may not limit fish abundance, competition for zooplankton could be a key process structuring fish distribution around reefs.

There may be value in exploring other explanations of the upstream preference, such as flow dynamics and its influence on the energetics of swimming (Chen et al. 2016). Many artificial reefs, including those we studied, are constructed with specific orientation and geometry intended to disrupt the flow of currents and generate a counter flow 'wake region' downstream (Oh et al. 2011). Disrupted flow generates eddies, which can cause aggregation of passively drifting zooplankton downstream of reef structures (Mann & Lazier 1996). This feature should make the downstream side of artificial reefs more attractive to zooplanktivores, yet our observations of an upstream preference refute this. On the upstream side, fish need only maintain their position while monitoring their reactive volume for prey drifting toward them (Kiflawi & Genin 1997). On the downstream side, turbulence may generate unstable flow patterns making it more energetically costly to maintain position or

forage. Thus, upstream preference may be an evolutionary adaptation to maximise net energy input.

In temperate regions, where large proportions of reef fish biomass are supported by pelagic subsidies (Truong et al. 2017, Udy et al. 2019, Zuercher & Galloway 2019, Holland et al. 2020), and where the direction of oceanic currents remains consistent over time, designed reefs arranged as linear arrays with the long axis positioned perpendicular to the prevailing current may be able to support increased local production (Champion et al. 2015). This configuration would increase the horizontal length of the leading edge of reef-associated schools, minimising impacts of localised depletion across the reef and enhancing the production of zooplanktivores (Champion et al. 2015). Incorporating enhanced vertical relief into artificial reef design may achieve a similar outcome, by extending the potential foraging space into the vertical dimension.

4.3. Accessing the water column

After sunrise, fish schools on the artificial reef field rose in the water column and expanded in vertical thickness so the tops of schools were 13 m above the seafloor, while at the nearby natural reef schools were only 8 m above the seafloor. This difference suggests that the additional vertical relief provided by the artificial reef (9 m) was used by schooling zooplanktivores to access a greater vertical extent of the water column. Alternatively, fish at the artificial reef may spread out vertically for better access prey due to the smaller horizontal footprint of the artificial reef field habitat relative to that of the natural reef.

We observed an analogous behaviour of association with vertical relief at natural reefs, as school probability of occurrence correlated positively with changes in bathymetry (Davis & Smith 2017). Predictions from our natural reefs model estimated only an 8% probability of school occurrence over completely flat seafloor, versus 37% for the maximum roughness we

observed. Fish likely take advantage of natural vertical relief because it allows them to feed higher in the water column, while maintaining proximity to refuge. As many schooling zooplanktivores maintain proximity to benthic structure for refuge from predators, there may exist a vertical gradient in predation pressure on zooplankton, with intense predation just above the seafloor (Motro et al. 2005). By providing additional vertical relief, far above what would typically be found on natural reefs, artificial reefs can overcome this limitation.

Alternatively, this behaviour may arise in response to the threat of predation. The artificial reefs in this region have been built to provide fishing opportunities for recreational anglers (Keller et al. 2016) and monitoring studies have found these reefs to be frequented by schools of *Seriola lalandi* (Scott et al. 2015, Becker et al. 2017), a voracious pelagic predator highly prized by anglers (Champion et al. 2018). In the presence of predators, prey fish often aggregate more densely (Johannes 1993), maintain proximity to benthic structure for refuge (Morgan & Godin 1985) or attempt to escape, however the latter option would require fish to venture into exposed habitat at the isolated artificial reef. Due to the limited horizontal extent and enhanced vertical relief of the artificial reef, prey fish may have to aggregate higher in the water column than they would at natural rocky reefs in the presence of predators.

Our observations of how schooling fish used the enhanced vertical relief across an artificial reef provides evidence for the effectiveness of simple vertical structures. The reef field included steel tower structures with small cross-braces, but no holes or internal refuges. These towers were sufficient to encourage fish to use a greater proportion of the water column. Simple modifications to reef design, through the inclusion of basic steel towers, may improve artificial habitat without significantly inflating material and installation costs. However, this should not diminish the importance of internal spaces incorporated into the

main structure, which are still an important feature for more benthic associated species (Sherman et al. 2002).

4.4. Nocturnal behaviour

The bulk of schooling fish recorded at the artificial reef field, and to a lesser degree at the nearby natural reef, exhibited demersal distribution at night and were settled near the seabed as a thin layer with wide horizontal extent. These fish aggregated and rose to midwater in the early morning. We did not observe a similar degree of nocturnal behaviour at the nearby natural reef. Since there were significant differences in fish community composition between the two sites, it is likely that this pattern is at least partially driven by the behaviour of *T. novaezelandiae*, and to a lesser extent *A. strigatus*, as they were the dominant species identified at the artificial reef during early morning. It is also important to note that the natural reef habitat was spread over a wider area with no clearly defined boundaries, making patterns in distribution potentially more difficult to detect. The artificial reef may have effectively concentrated these behaviours to occur within a smaller area, since fish had no suitable adjacent habitat to travel to at night. Further, owing to the complex bathymetry of natural rocky reefs it is likely that many demersal schools went undetected by our survey methods as they were settled at night along the seafloor, within canopy-forming macroalgae or under rock overhangs.

Some reef zooplanktivores have been observed to feed at night (Gladfelter 1979), suggesting that these nocturnal demersal distributions may have resulted from fish feeding on epi-benthic zooplankton as they emerged from or returned to the benthic substrate (Galzin 1987, Myers et al. 2016). This is more likely at the natural reef, as highly abundant nocturnal species, such as *Pempheris affinis* and *P. multiradiata*, emerge to feed on zooplankton at night (Annese & Kingsford 2005). Due to their diurnal distribution under natural rock

overhangs, they would be absent from our remote video deployments. Alternatively, schooling zooplanktivores may assume this distribution at dusk, while light levels are sufficient to facilitate aggregation, and maintain their relative positions throughout the night in the absence of visual cues. This would provide a means of conserving energy at night while minimising individual predation risk. Moored in-situ echosounders might be able to document this kind of behaviour (Fabi & Sala 2002, Sala et al. 2007).

These patterns we observed before and after sunrise represent just two instances in a 24-hour cycle, and as such they may only be representative of the times of observation. For example, Sala et al. (2007) observed the greatest density of fish at an artificial reef late at night and in the early morning, but very low densities in the afternoon. To properly understand diel behaviour it may be necessary to observe fish distribution over 24-hour cycles with finer temporal resolution (Myers et al. 2016).

Regardless of whether fish used the artificial reef field at night to feed or to rest, the arrangement of multiple modules at JDN to form a reef field (rather than a single isolated structure at the OAR) likely facilitated this pattern and may contribute to supporting larger abundances of these fish (Becker et al. 2019). In terms of reef design, to support greater abundances of schooling zooplanktivores it may be necessary to find a compromise in module layout that achieves this reef field effect, without excessively 'shadowing' downstream modules.

4.5. Conclusion

By investigating fine scale patterns in the distribution of schooling zooplanktivores around temperate reefs we have highlighted important behavioural responses to benthic structure, water currents and diel period. These insights into the behaviour of schooling zooplanktivores can be used to inform enhanced artificial reef designs for improving the sustainability of

coastal fisheries. Our main findings indicate that reefs with large vertical relief provide desirable habitat for zooplanktivores, and reefs positioned in the path of prevailing currents will enhance the potential influence of planktonic subsidies. The nocturnal behaviour we observed also indicates the potential for benthopelagic trophic coupling (Puckeridge et al. 2021). More research relying on in-situ sampling of zooplankton at multiple distances to reef structures is required to validate whether the behaviours we observed correspond with actual gradients in zooplankton density, and even more importantly, in individual consumption rates.

Acknowledgements

Many thanks to the dedicated volunteers and SIMS staff who helped with data collection and to skipper, John Paton for the many late nights at sea. Thanks to Hayley Bates (Echoview) for her help in developing the dataflow for processing the MBES data in Echoview. This work was funded by an Australian Government Research Training Program Scholarship. IMS and JDE were supported by the ARC (LP120100592, DP150102656 and DP190102293).

Literature cited

Anderson TW, Sabado BD (1995) Correspondence between food availability and growth of a planktivorous temperate reef fish. Journal of Experimental Marine Biology and Ecology 189:65-76

Annese DM, Kingsford MJ (2005) Distribution, movements and diet of nocturnal fishes on temperate reefs. Environmental Biology of Fishes 72:161-174

Bakun A (2006) Wasp-waist populations and marine ecosystem dynamics: navigating the "predator pit" topographies. Progress in oceanography 68:271-288

Basford AJ, Feary DA, Truong G, Steinberg PD, Marzinelli EM, Vergés A (2016) Feeding habits of range-shifting herbivores: tropical surgeonfishes in a temperate environment. Marine and Freshwater Research 67:75-83

Becker A, Taylor MD, Lowry MB (2017) Monitoring of reef associated and pelagic fish communities on Australia's first purpose built offshore artificial reef. ICES Journal of Marine Science 74:277-285

Becker A, Smith JA, Taylor MD, McLeod J, Lowry MB (2019) Distribution of pelagic and epi-benthic fish around a multi-module artificial reef-field: Close module spacing supports a connected assemblage. Fisheries Research 209:75-85

Borland HP, Gilby BL, Henderson CJ, Leon JX and others (2021) The influence of seafloor terrain on fish and fisheries: A global synthesis. Fish and Fisheries

Bray RN (1980) Influence of water currents and zooplankton densities on daily foraging movements of blacksmith, Chromis punctipinnis, a planktivorous reef fish. FISH BULL(SEATTLE) 78:829-841

Campbell MD, Pollack AG, Gledhill CT, Switzer TS, DeVries DA (2015) Comparison of relative abundance indices calculated from two methods of generating video count data. Fisheries Research 170:125-133

Champion C, Suthers IM, Smith JA (2015) Zooplanktivory is a key process for fish production on a coastal artificial reef. Marine Ecology Progress Series 541:1-14

Champion C, Hobday AJ, Zhang X, Pecl GT, Tracey SR (2018) Changing windows of opportunity: past and future climate-driven shifts in temporal persistence of kingfish (*Seriola lalandi*) oceanographic habitat within south-eastern Australian bioregions. Marine and Freshwater Research 70:33-42

Chen S-Y, Fei Y-HJ, Chen Y-C, Chi K-J, Yang J-T (2016) The swimming patterns and energy-saving mechanism revealed from three fish in a school. Ocean Engineering 122:22-31

Claisse JT, Pondella DJ, Love M, Zahn LA, Williams CM, Williams JP, Bull AS (2014) Oil platforms off California are among the most productive marine fish habitats globally. Proceedings of the National Academy of Sciences 111:15462-15467

Colbo K, Ross T, Brown C, Weber T (2014) A review of oceanographic applications of water column data from multibeam echosounders. Estuarine, coastal and shelf science 145:41-56

Davis TR, Smith SD (2017) Proximity effects of natural and artificial reef walls on fish assemblages. Regional Studies in Marine Science 9:17-23

Dawson G, Suthers IM, Brodie S, Smith JA (2020) The bioenergetics of a coastal forage fish: Importance of empirical values for ecosystem models. Deep Sea Research Part II: Topical Studies in Oceanography 175:104700

Docmac F, Araya M, Hinojosa IA, Dorador C, Harrod C (2017) Habitat coupling writ large: pelagic-derived materials fuel benthivorous macroalgal reef fishes in an upwelling zone. Ecology 98:2267-2272

Elith J, H. Graham C, P. Anderson R, Dudík M and others (2006) Novel methods improve prediction of species' distributions from occurrence data. Ecography 29:129-151

Fabi G, Sala A (2002) An assessment of biomass and diel activity of fish at an artificial reef (Adriatic Sea) using a stationary hydroacoustic technique. ICES Journal of Marine Science 59:411-420

Forrester GE (1991) Social rank, individual size and group composition as determinants of food consumption by humbug damselfish, Dascyllus aruanus. Animal Behaviour 42:701-711

Froese R, and, Pauly D (2009) FishBase: a global information system on fishes. International Center for Living Aquatic Resources Management

Gal G (1993) The interactions between topography, currents and zooplankton. Hebrew University, the curriculum of oceanography and the H. Steinitz Marine …

Galzin R (1987) Structure of fish communities of French Polynesian coral reefs. 11. Temporal Scales. Mar Ecol Prog Ser 41:137-145

Gladfelter W (1979) Twilight migrations and foraging activities of the copper sweeper Pempheris schomburgki (Teleostei: Pempheridae). Marine Biology 50:109-119

Hamner W, Jones M, Carleton J, Hauri I, Williams DM (1988) Zooplankton, planktivorous fish, and water currents on a windward reef face: Great Barrier Reef, Australia. Bulletin of Marine Science 42:459-479

Hijmans RJ (2020) raster: Geographic Data Analysis and Modeling. R package version 3.3-13

Hobson ES, Chess JR (1978) Trophic relationships among fishes and plankton in the lagoon at Enewetak Atoll, Marshall Islands. Fish Bull 76:133-153

Holland MM, Smith JA, Everett JD, Vergés A, Suthers IM (2020) Latitudinal patterns in trophic structure of temperate reef-associated fishes and predicted consequences of climate change. Fish and Fisheries 21:1092-1108

Holland MM, Becker A, Smith JA, Everett JD, Suthers IM (2021) Characterizing the three-dimensional distribution of schooling reef fish with a portable multibeam echosounder. Limnology and Oceanography: Methods

Holzman R, Reidenbach MA, Monismith SG, Koseff JR, Genin A (2005) Near-bottom depletion of zooplankton over a coral reef II: relationships with zooplankton swimming ability. Coral Reefs 24:87-94

Johannes MR (1993) Prey aggregation is correlated with increased predation pressure in lake fish communities. Canadian Journal of Fisheries and Aquatic Sciences 50:66-73

Keller K, Steffe AS, Lowry M, Murphy JJ, Suthers IM (2016) Monitoring boat-based recreational fishing effort at a nearshore artificial reef with a shore-based camera. Fisheries Research 181:84-92

Kiflawi M, Genin A (1997) Prey flux manipulation and the feeding rates of reef-dwelling planktivorous fish. Ecology 78:1062-1077

Kingsford M, MacDiarmid A (1988) Interrelations between planktivorous reef fish and zooplankton in temperate waters. Marine ecology progress series Oldendorf 48:103-117

Lumpkin R, Özgökmen T, Centurioni L (2017) Advances in the application of surface drifters. Annual review of marine science 9:59-81

Mann K, Lazier J (1996) Dynamics of Marine Ecosystems 3rd edn: Part B–Vertical Structure in Coastal Waters: Coastal Upwelling Regions, Vol. Blackwell Publishing

Misund OA, Aglen A, Frønæs E (1995) Mapping the shape, size, and density of fish schools by echo integration and a high-resolution sonar. ICES Journal of Marine Science: Journal du Conseil 52:11-20

Moore SK, Suthers IM (2006) Evaluation and correction of subresolved particles by the optical plankton counter in three Australian estuaries with pristine to highly modified catchments. Journal of Geophysical Research: Oceans 111

Morais RA, Bellwood DR (2019) Pelagic Subsidies Underpin Fish Productivity on a Degraded Coral Reef. Curr Biol 29:1521-1527 e1526

Morgan MJ, Godin JGJ (1985) Antipredator benefits of schooling behaviour in a cyprinodontid fish, the banded killifish (*Fundulus diaphanus*). Zeitschrift für Tierpsychologie 70:236-246

Motro R, Ayalon I, Genin A (2005) Near-bottom depletion of zooplankton over coral reefs: III: vertical gradient of predation pressure. Coral Reefs 24:95-98

Myers EM, Harvey ES, Saunders BJ, Travers MJ (2016) Fine-scale patterns in the day, night and crepuscular composition of a temperate reef fish assemblage. Marine Ecology 37:668-678

Niku J, Brooks W, Herliansyah R, Hui FK, Taskinen S, Warton DI (2020) gllvm: Generalized Linear Latent Variable Models. R package version 1.2.2 Methods in Ecology and Evolution

NSW Department of Planning Industry and Environment (2018) NSW Marine LiDAR Topo-Bathy 2018 Geotif

O'Brien WJ (1979) The predator-prey interaction of planktivorous fish and zooplankton: recent research with planktivorous fish and their zooplankton prey shows the evolutionary thrust and parry of the predator-prey relationship. American Scientist 67:572-581

Oh TG, Otake S, Lee MO (2011) Estimating the effective wake region (current shadow) of artificial reefs. In: Artificial Reefs in Fisheries Management. CRC Press Boca Raton, FL, USA, p 279-295

Paxton AB, Taylor JC, Peterson C, Fegley SR, Rosman JH (2019) Consistent spatial patterns in multiple trophic levels occur around artificial habitats. Marine Ecology Progress Series 611:189-202

Pikitch EK, Rountos KJ, Essington TE, Santora C and others (2014) The global contribution of forage fish to marine fisheries and ecosystems. Fish and Fisheries 15:43-64

Prandle D, Matthews J (1990) The dynamics of nearshore surface currents generated by tides, wind and horizontal density gradients. Continental Shelf Research 10:665-681

Puckeridge AC, Becker A, Taylor MD, Lowry MB, McLeod J, Schilling HT, Suthers IM (2021) Foraging behaviour and movements of an ambush predator reveal benthopelagic coupling on artificial reefs. Marine Ecology Progress Series 666:171-182

R Core Team (2020) R: A language and environment for statistical computing. R Foundation for Statistical Computing, Vienna, Austria

Reid D, Simmonds E (1993) Image analysis techniques for the study of fish school structure from acoustic survey data. Canadian Journal of Fisheries and Aquatic Sciences 50:886-893

Rilov G, Benayahu Y (2000) Fish assemblage on natural versus vertical artificial reefs: the rehabilitation perspective. Marine Biology 136:931-942

Rilov G, Benayahu Y (2002) Rehabilitation of coral reef-fish communities: the importance of artificial-reef relief to recruitment rates. Bulletin of marine Science 70:185-197

Sala A, Fabi G, Manoukian S (2007) Vertical diel dynamic of fish assemblage associated with an artificial reef (Northern Adriatic Sea). Scientia Marina 71:355-364

Sandin SA, Pacala SW (2005) Demographic theory of coral reef fish populations with stochastic recruitment: comparing sources of population regulation. Am Nat 165:107-119

Scott ME, Smith JA, Lowry MB, Taylor MD, Suthers IM (2015) The influence of an offshore artificial reef on the abundance of fish in the surrounding pelagic environment. Marine and Freshwater Research 66:429-437

Sheehan EV, Bridger D, Nancollas SJ, Pittman SJ (2020) PelagiCam: a novel underwater imaging system with computer vision for semi-automated monitoring of mobile marine fauna at offshore structures. Environmental Monitoring and Assessment 192:11

Sherman RL, Gilliam DS, Spieler RE (2002) Artificial reef design: void space, complexity, and attractants. ICES Journal of Marine Science 59:S196-S200

Skinner C, Mill A, Fox M, Newman S, Zhu Y, Kuhl A, Polunin N (2021) Offshore pelagic subsidies dominate carbon inputs to coral reef predators. Science Advances 7:eabf3792

Smith JA, Cornwell WK, Lowry MB, Suthers IM (2017) Modelling the distribution of fish around an artificial reef. Marine and Freshwater Research 68:1955-1964

Suthers IM, Taggart C, Rissik D, Baird M (2006) Day and night ichthyoplankton assemblages and zooplankton biomass size spectrum in a deep ocean island wake. Marine Ecology Progress Series 322:225-238

Truong L, Suthers IM, Cruz DO, Smith JA (2017) Plankton supports the majority of fish biomass on temperate rocky reefs. Marine biology 164:73

Udy J, Wing S, Connell-Milne SO, Durante L, McMullin R, Kolodzey S, Frew R (2019) Regional differences in supply of organic matter from kelp forests drive trophodynamics of temperate reef fish. Marine Ecology Progress Series 621:19-32

Weber TC, Peña H, Jech JM (2009) Consecutive acoustic observations of an Atlantic herring school in the Northwest Atlantic. ICES Journal of Marine Science 66:1270-1277

Wilson MF, O'Connell B, Brown C, Guinan JC, Grehan AJ (2007) Multiscale terrain analysis of multibeam bathymetry data for habitat mapping on the continental slope. Marine Geodesy 30:3-35

Yahel R, Yahel G, Berman T, Jaffe JS, Genin A (2005a) Diel pattern with abrupt crepuscular changes of zooplankton over a coral reef. Limnology and Oceanography 50:930-944

Yahel R, Yahel G, Genin A (2005b) Near-bottom depletion of zooplankton over coral reefs: I: diurnal dynamics and size distribution. Coral reefs 24:75-85

Zuercher R, Galloway AW (2019) Coastal marine ecosystem connectivity: pelagic ocean to kelp forest subsidies. Ecosphere 10:e02602

Figure captions

Figure 1 The locations of the three artificial (▼) and five natural (◆) reef sites used to study fish school distribution (■) and characteristics (■) and their general location in Australia (●). Shaded panels with contours indicate bathymetry and structures of the eight corresponding site locations. The outlines of artificial reef structures (panels: OAR, AM and JDN) are also indicated, with OAR indicating the position of concrete anchor blocks (■) and the steel reef structure (□), AM indicating the position of the shipwreck lying on its side, and JDN indicating the position of concrete modules with (▲) and without towers (●). Contours on main chart indicate a 25 m change in bathymetry while contours on panels indicate a 2 m change.

Figure 2 Gridded school thickness for four survey dates at the SS Annie Miller (AM – top row) and Sydney Offshore Artificial Reef (OAR – bottom row). White vectors extending from the origin of each raster represent the current over a 5-minute period. Reef structures are displayed as pink polygons for each panel.

Figure 3 Covariate coefficient plot generated from the Generalised Linear Latent Variable Model (GLLVM), indicating mean values (red dots) and confidence intervals for the effect of reef site on the abundance of the five schooling species detected. Images obtained from efishalbum.com.

Figure 4 Ordination plot output for the two-variable generalised linear latent variable model of relative fish abundance. Points are coloured by reef site and the ellipses represent 95% confidence intervals for each of the two reef sites (N5 natural, JDN artificial), showing the greater range in variability at the natural reef. Symbols represent the survey dates when video footage was collected.

Figure 5 GLS model effects plots of underwater video data, displaying mean values (symbols) and 95% confidence intervals for the interaction of reef site with total fish abundance (a), species richness (b), and Shannon diversity index (c) for the natural reef (N5) and nearby artifical reef modules (JDN). Raw data values for each factor have been jittered to aid visualisation. Asterisks above each panel indicate significance level (*: $p < 0.05$, **: $p < 0.01$, ***: $p < 0.001$).

Figure 6 Partial effects from the artificial reef model (a, b, c, d) and the natural reef model (e, f, g, h), estimating probability of occurrence of a fish school (derived from the 'school thickness' data), showing the fixed effect of the two artificial reef sites (a), four survey dates (b), 'distance' from the artificial reef (c) 'relative bearing' from the artificial reef (d; 0 = downstream, 1 = upstream), the fixed effect of the four natural reef sites (e), five survey dates (f), seafloor 'roughness' (g) and 'relative aspect' (h; 0 = minimum exposure, 1 = maximum exposure). Error bars in and ribbons represent 95% confidence intervals. Rug plots for the x-axes indicate the distribution of the raw data used to create the two models.

Figure 7 Predicted probability of fish school occurrence (red line) from the artificial reef GLM. The artificial reef is illustrated by the grey structure, and the black vector represents the direction of current flow. The ribbon represents standard error of the mean.

Figure 8 GLS model effects displaying mean values (symbols) and 95% confidence intervals for the interaction of reef site (N5 natural, JDN artificial) and diel period (night: blue and day: red) with variables describing school characteristics, including area of an individual school (a), proportion of surveyed area containing schools (b), volume of individual schools (c), number of schools per hectare of area surveyed (d), school height above the seafloor (e), school thickness, or the sum of each 1 m depth interval containing fish (f), perimeter to area ratio (g), area to volume ratio (h) and horizontal distance from the reef centre (i). Significant fixed effects (Site, Diel) or variable interactions (Site:Diel) are indicated above each panel, along with significance level (*: $p < 0.05$, **: $p < 0.01$, ***: $p < 0.001$). Raw data are included for each combination of factors. Note, all models also contain a fixed effect for survey date to account for day-to-day variability (not shown).

Tables

Table 1 Site names, locations and descriptions, and the aims they were used to address.

Site	Reef type	Coordinates	Survey	Aims	Name and year of deployment	Survey dates	Site description	Data
OAR	Artificial	33.8466° S 151.2998° E	School distribution	1	Sydney Offshore Artificial Reef, 2011	23/10/2018 06/11/2018 19/11/2018 21/01/2019	Singular steel lattice structure with two towers Structure height: 4 m Total height: 12 m Mean depth: 36 m	Multibeam acoustics Remote underwater video Drifter coordinates
AM	Artificial	33.8666° S 151.2984° E	School distribution	1	SS Annie M Miller, 1929	23/10/2018 06/11/2018 19/11/2018 21/01/2019	48 m long historic shipwreck Structure height: 5 m Mean depth: 42 m	Multibeam acoustics Remote underwater video Drifter coordinates
N1	Natural	33.8492° S 151.2942° E	School distribution	1	NA	23/10/2018 06/11/2018 19/11/2018 21/01/2019	Mean depth: 26 m Min depth: 20 m Max depth: 32.5 m	Multibeam acoustics Remote underwater video Drifter coordinates

Site	Reef type	Coordinates	Survey	Aims	Name and year of deployment	Survey dates	Site description	Data
N2	Natural	33.9410° S 151.2751° E	School distribution	1	NA	23/10/2018 06/11/2018 19/11/2018 05/12/2018	Mean depth: 34 m Min depth: 30.5 m Max depth: 38 m	Multibeam acoustics Remote underwater video Drifter coordinates
N3	Natural	33.9588° S 151.2685° E	School distribution	1	NA	23/10/2018 06/11/2018 19/11/2018 05/12/2018	Mean depth: 27.5 m Min depth: 18.5 m Max depth: 34.5 m	Multibeam acoustics Remote underwater video Drifter coordinates
N4	Natural	33.9728° S 151.2681° E	School distribution	1	NA	23/10/2018 06/11/2018 19/11/2018 05/12/2018	Mean depth: 33 m Min depth: 28 m Max depth: 39 m	Multibeam acoustics Remote underwater video Drifter coordinates

Site	Reef type	Coordinates	Survey	Aims	Name and year of deployment	Survey dates	Site description	Data
JDN	Artificial	34.0943° S 151.1776° E	Diel effects on school characteristics	2, 3	John Dunphy Reef, North cluster, 2017	14/08/2019 03/09/2019 26/09/2019 31/10/2019 08/11/2019 18/08/2020 28/08/2020	Five clusters of pre-formed concrete modules. One tower per cluster Total height: 9 m Structure height: 5 m Mean depth: 29 m	Multibeam acoustics Remote underwater video Vessel coordinates Zooplankton net samples
N5	Natural	34.0756° S 151.1824° E	Diel effects on school characteristics	2, 3	NA	14/08/2019 03/09/2019 26/09/2019 31/10/2019 08/11/2019 18/08/2020 28/08/2020	Mean depth: 25.5 m Min depth: 20.5 m Max depth: 27.5 m	Multibeam acoustics Remote underwater video Vessel coordinates Zooplankton net samples

1

Table 2 Results for the binomial GLMs describing the distribution of schooling fish around artificial and natural reefs. Model terms are as follows: Presence – grid cell with fish detected (1) or no fish detected (0), reef_site – a factor for the individual reef sites, cell_dist – cell distance (in m) from the reef centre, rel_bear – bearing of cell from the reef centroid relative to prevailing current, rough – seafloor roughness (m), rel_asp – relative exposure of bathymetry aspect to the prevailing current. Columns are as follows: R df – residual degrees of freedom, N-R dev – difference between null and residual deviance, ΔAIC null – ΔAIC between the full model and an intercept-only model, ΔAIC reef site – ΔAIC between the full model and a model containing only the reef site term, AUC – area under the curve. Significance level of Pr(>|z|) indicated by .: > 0.05, *: ≤ 0.05, **: ≤ 0.01, ***: ≤ 0.001, ****: ≤ 0.0001.

Model	GLM formula	R df	N-R dev	ΔAIC null	ΔAIC reef site	AUC	Predictor	Estimate	SE	z value	Pr(>|z|)	
Artificial	Presence ~ reef_site + date + cell_dist + rel_bear	12793	4749	4737	4727	0.88	intercept	-0.320	0.103	-3.115	<0.01	**
							reef_site OAR	-0.220	0.052	-4.206	<0.0001	****
							date 2018-11-06	0.163	0.096	1.695	0.090	.
							date 2018-11-19	3.351	0.088	38.201	<0.0001	****
							date 2019-01-21	1.587	0.086	18.527	<0.0001	****
							cell_dist	-0.044	0.001	-40.613	<0.0001	****
							rel_bear	1.356	0.092	14.664	<0.0001	****

Model	GLM formula	R df	N-R dev	ΔAIC null	ΔAIC reef site	AUC	Predictor	Estimate	SE	z value	Pr(>|z|)	
Natural	Presence ~ reef_site + date + rough + rel_asp	25439	2756	2738	1798	0.76	intercept	-3.017	0.084	-35.947	<0.0001	****
							reef_site N2	-0.615	0.056	-10.904	<0.0001	****
							reef_site N3	-2.130	0.072	-29.556	<0.0001	****
							reef_site N4	-1.424	0.063	-22.638	<0.0001	****
							date 2018-11-06	0.971	0.077	12.634	<0.0001	****
							date 2018-11-19	1.708	0.072	23.592	<0.0001	****
							date 2018-12-05	2.416	0.078	30.838	<0.0001	****
							date 2019-01-21	1.230	0.089	13.696	<0.0001	****
							rough	0.350	0.018	19.012	<0.0001	****
							rel_asp	0.240	0.071	3.364	<0.001	***

1

Figures

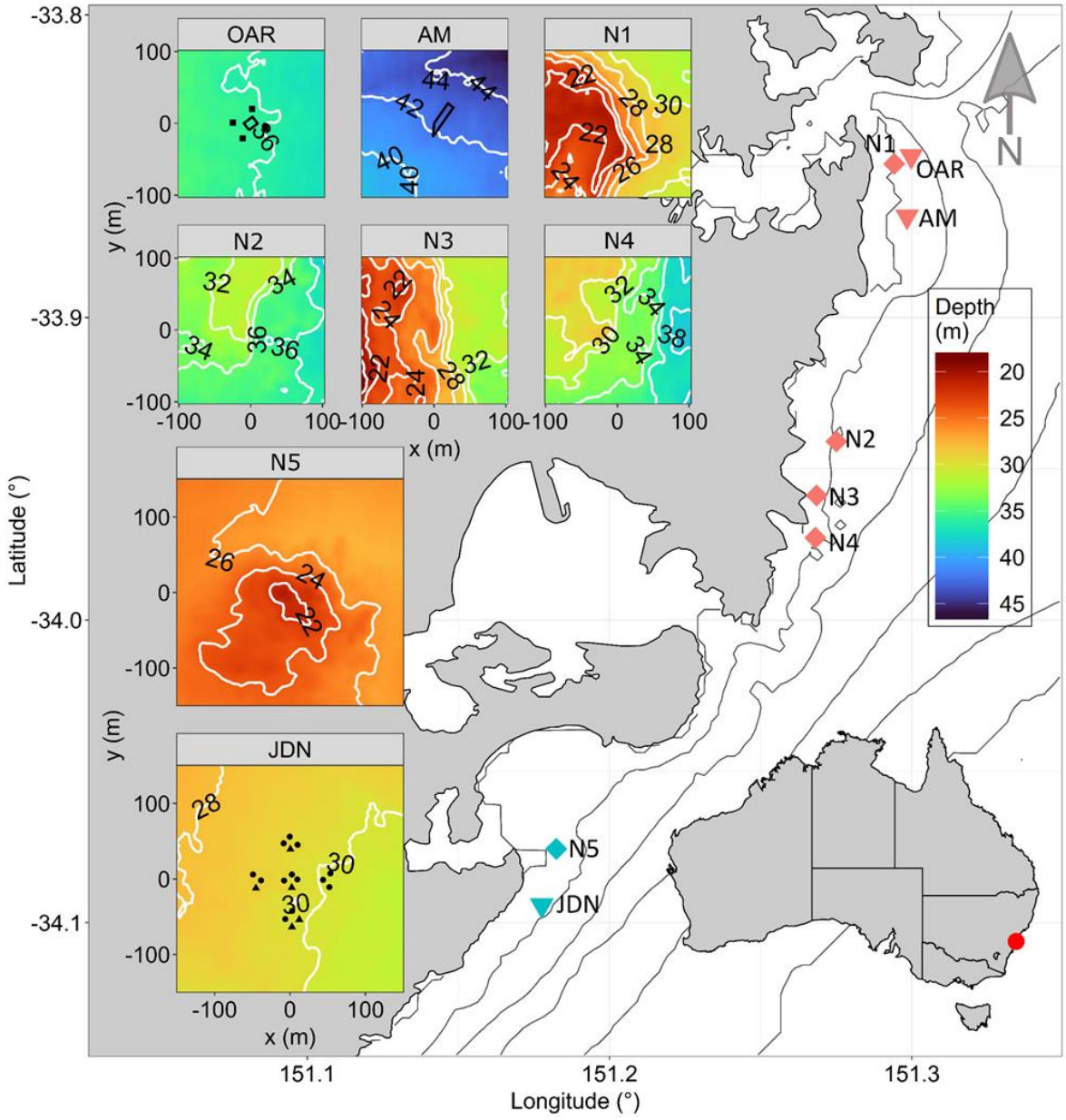

Figure 1 The locations of the three artificial (▼) and five natural (◆) reef sites used to study fish school distribution (■) and characteristics (■) and their general location in Australia (●). Shaded panels with contours indicate bathymetry and structures of the eight corresponding site locations. The outlines of artificial reef structures (panels: OAR, AM and JDN) are also indicated, with OAR indicating the position of concrete anchor blocks (■) and the steel reef structure (□), AM indicating the position of the shipwreck lying on its side, and JDN indicating the position of concrete modules with (▲) and without towers (●). Contours on main chart indicate a 25 m change in bathymetry while contours on panels indicate a 2 m change.

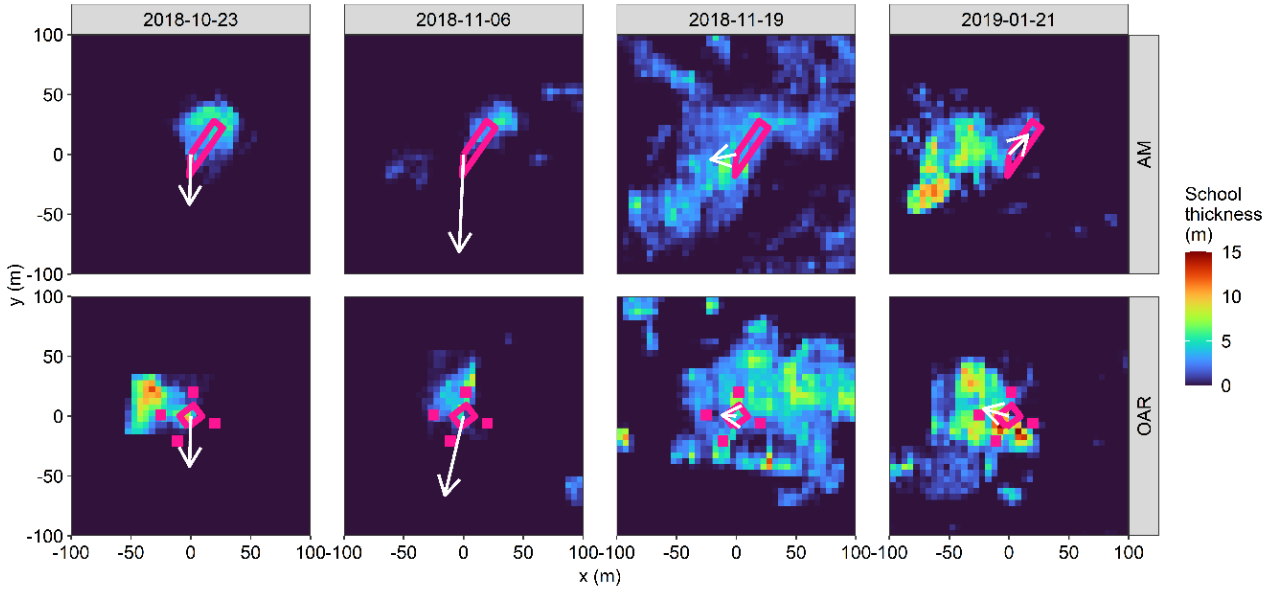

Figure 2 Gridded school thickness for four survey dates at the SS Annie Miller (AM – top row) and Sydney Offshore Artificial Reef (OAR – bottom row). White vectors extending from the origin of each raster represent the current over a 5-minute period. Reef structures are displayed as pink polygons for each panel.

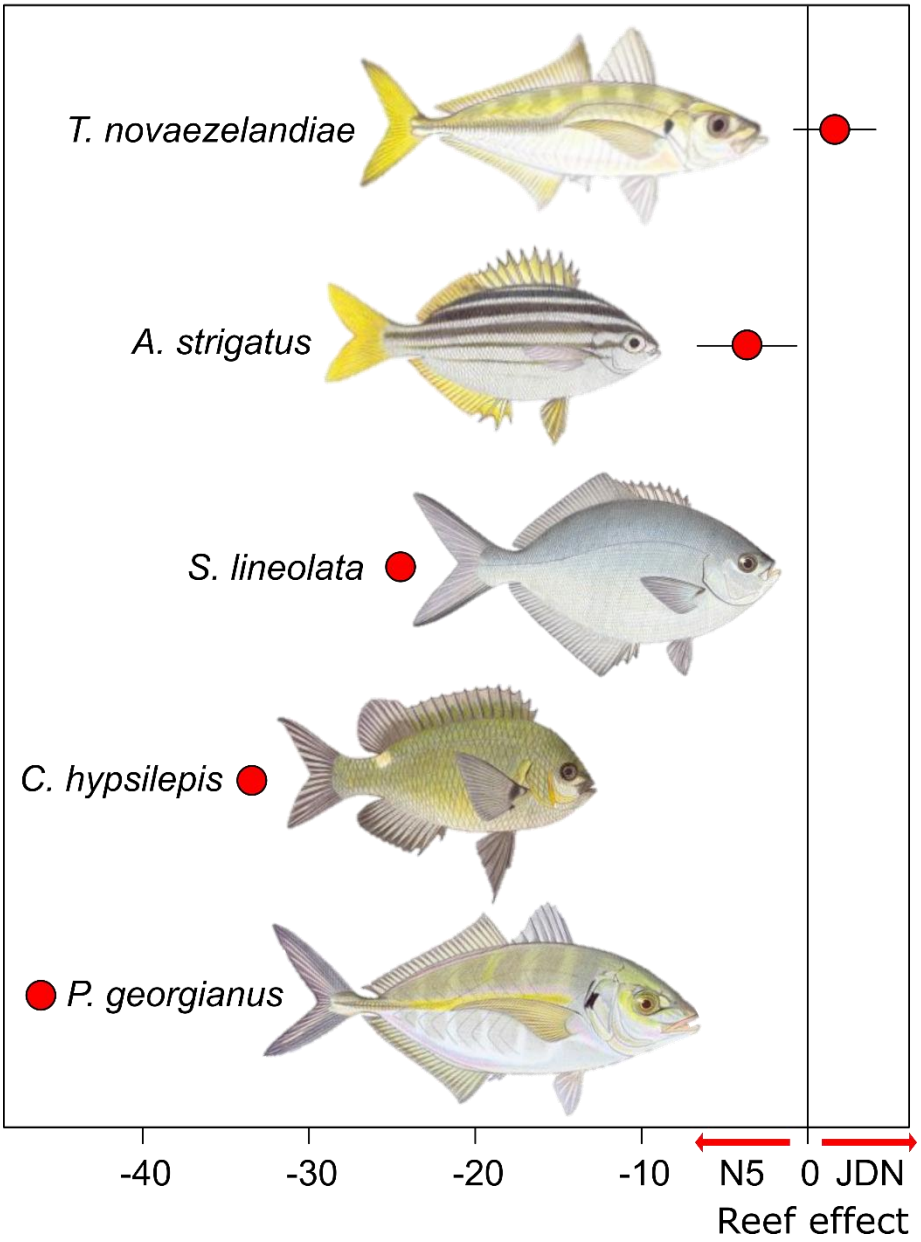

Figure 3 Covariate coefficient plot generated from the Generalised Linear Latent Variable Model (GLLVM), indicating mean values (red dots) and confidence intervals for the effect of reef site on the abundance of the five schooling species detected. Images obtained from efishalbum.com.

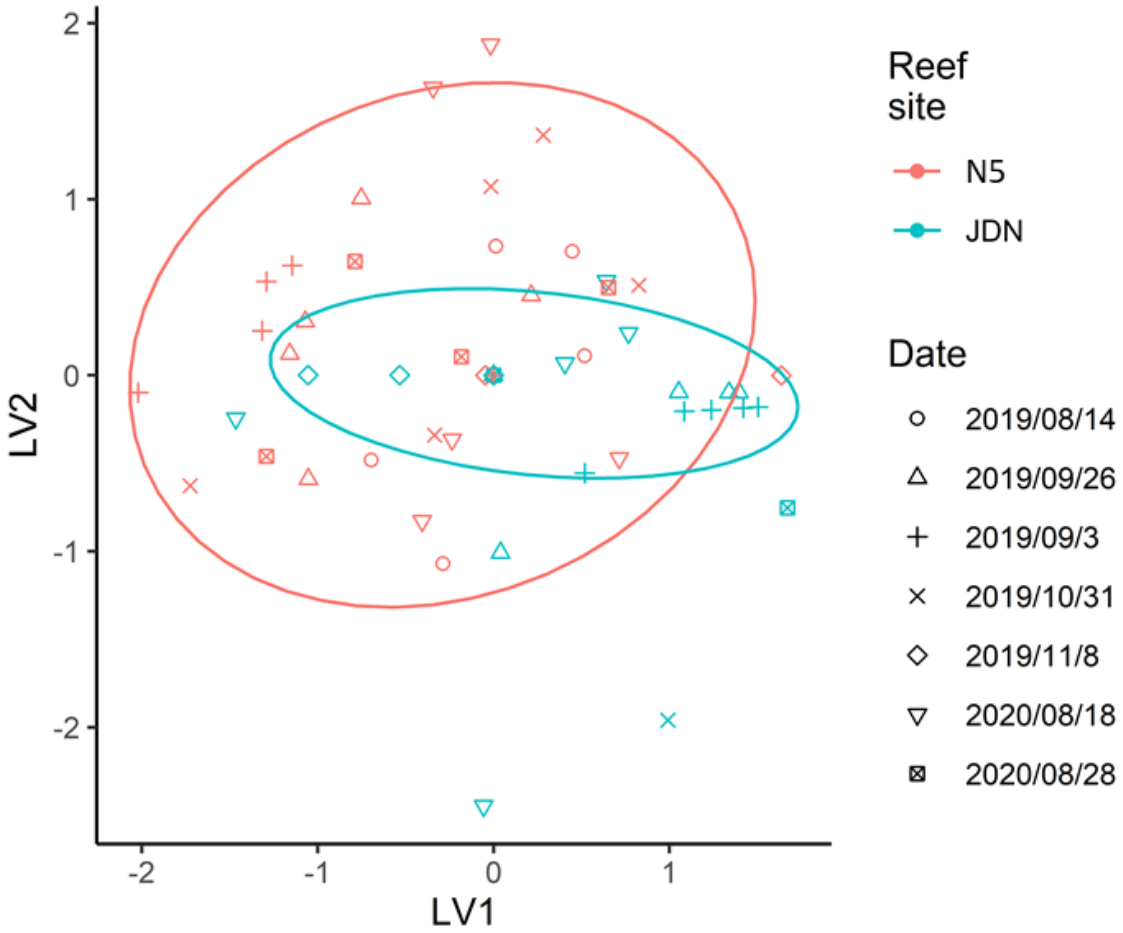

Figure 4 Ordination plot output for the two-variable generalised linear latent variable model of relative fish abundance. Points are coloured by reef site and the ellipses represent 95% confidence intervals for each of the two reef sites (N5 natural, JDN artificial), showing the greater range in variability at the natural reef. Symbols represent the survey dates when video footage was collected.

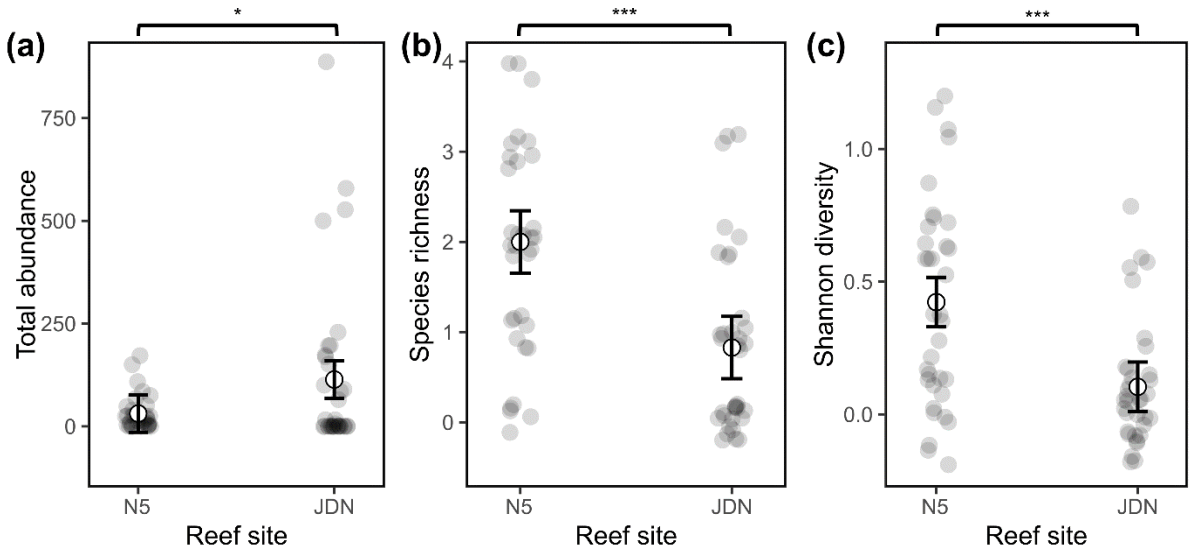

Figure 5 GLS model effects plots of underwater video data, displaying mean values (symbols) and 95% confidence intervals for the interaction of reef site with total fish abundance (a), species richness (b), and Shannon diversity index (c) for the natural reef (N5) and nearby artifical reef modules (JDN). Raw data values for each factor have been jittered to aid visualisation. Asterisks above each panel indicate significance level (*: $p < 0.05$, **: $p < 0.01$, ***: $p < 0.001$).

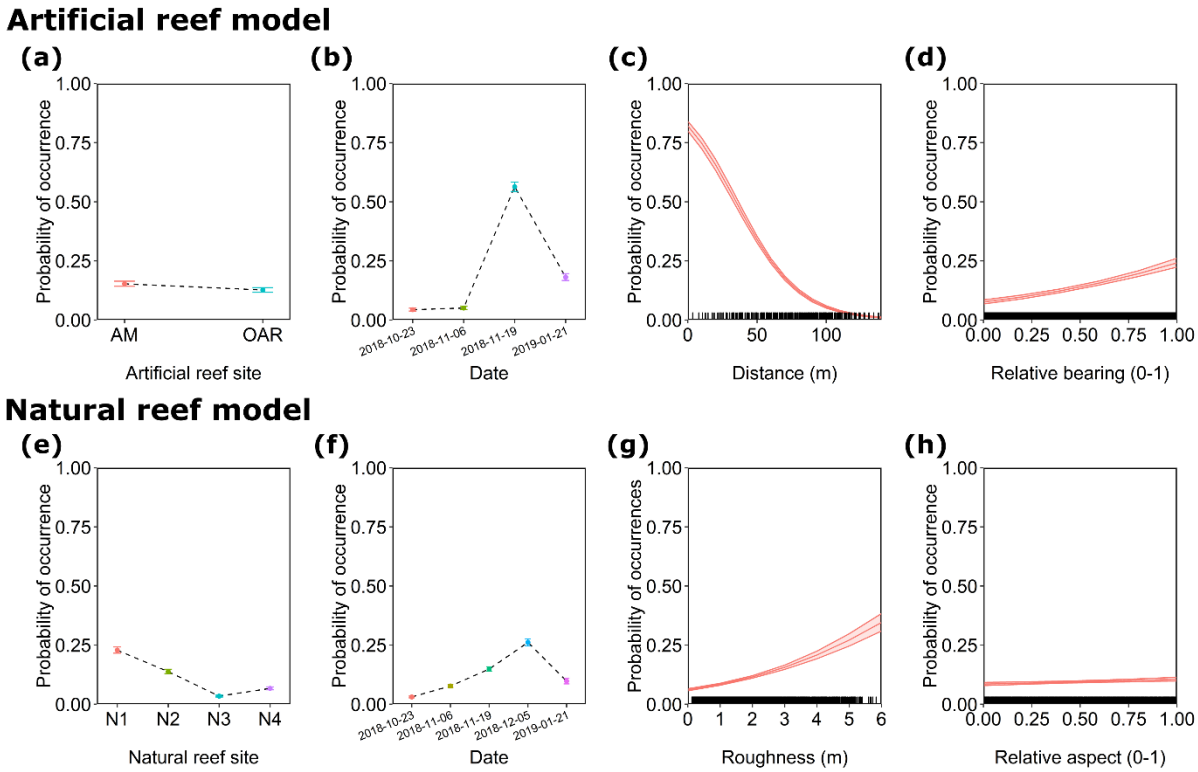

Figure 6 Partial effects from the artificial reef model (a, b, c, d) and the natural reef model (e, f, g, h), estimating probability of occurrence of a fish school (derived from the 'school thickness' data), showing the fixed effect of the two artificial reef sites (a), four survey dates (b), 'distance' from the artificial reef (c) 'relative bearing' from the artificial reef (d; 0 = downstream, 1 = upstream), the fixed effect of the four natural reef sites (e), five survey dates (f), seafloor 'roughness' (g) and 'relative aspect' (h; 0 = minimum exposure, 1 = maximum exposure). Error bars in and ribbons represent 95% confidence intervals. Rug plots for the x-axes indicate the distribution of the raw data used to create the two models.

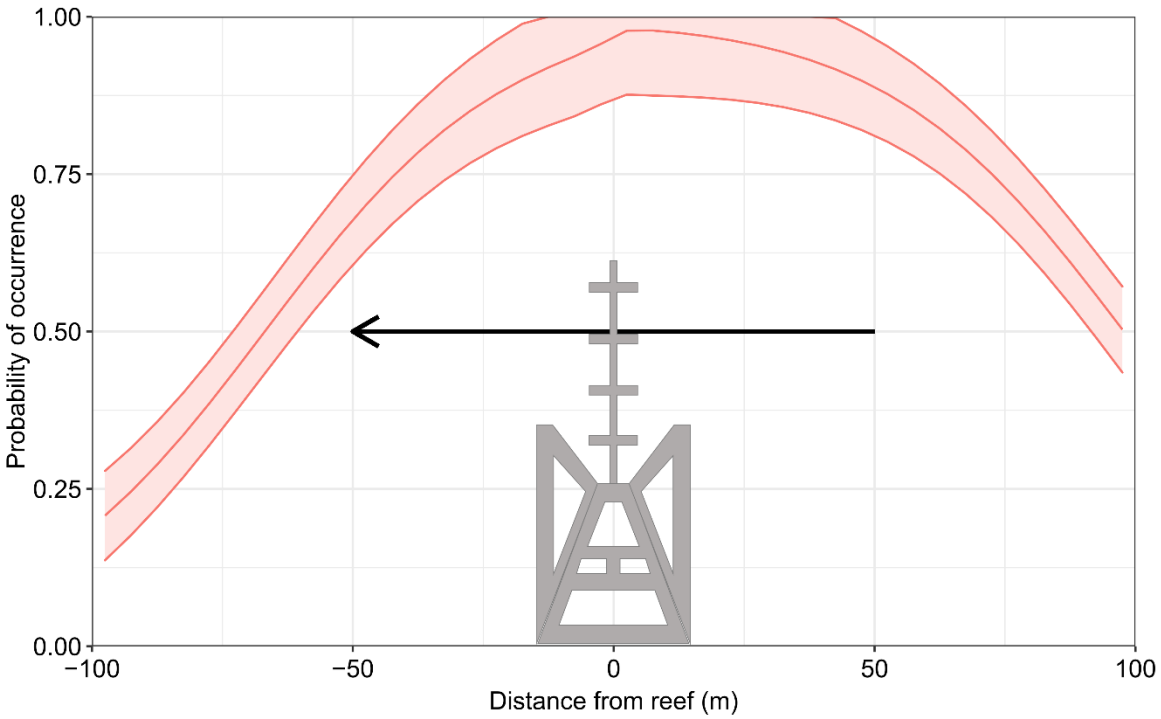

Figure 7 Predicted probability of fish school occurrence (red line) from the artificial reef GLM. The artificial reef is illustrated by the grey structure, and the black vector represents the direction of current flow. The ribbon represents standard error of the mean.

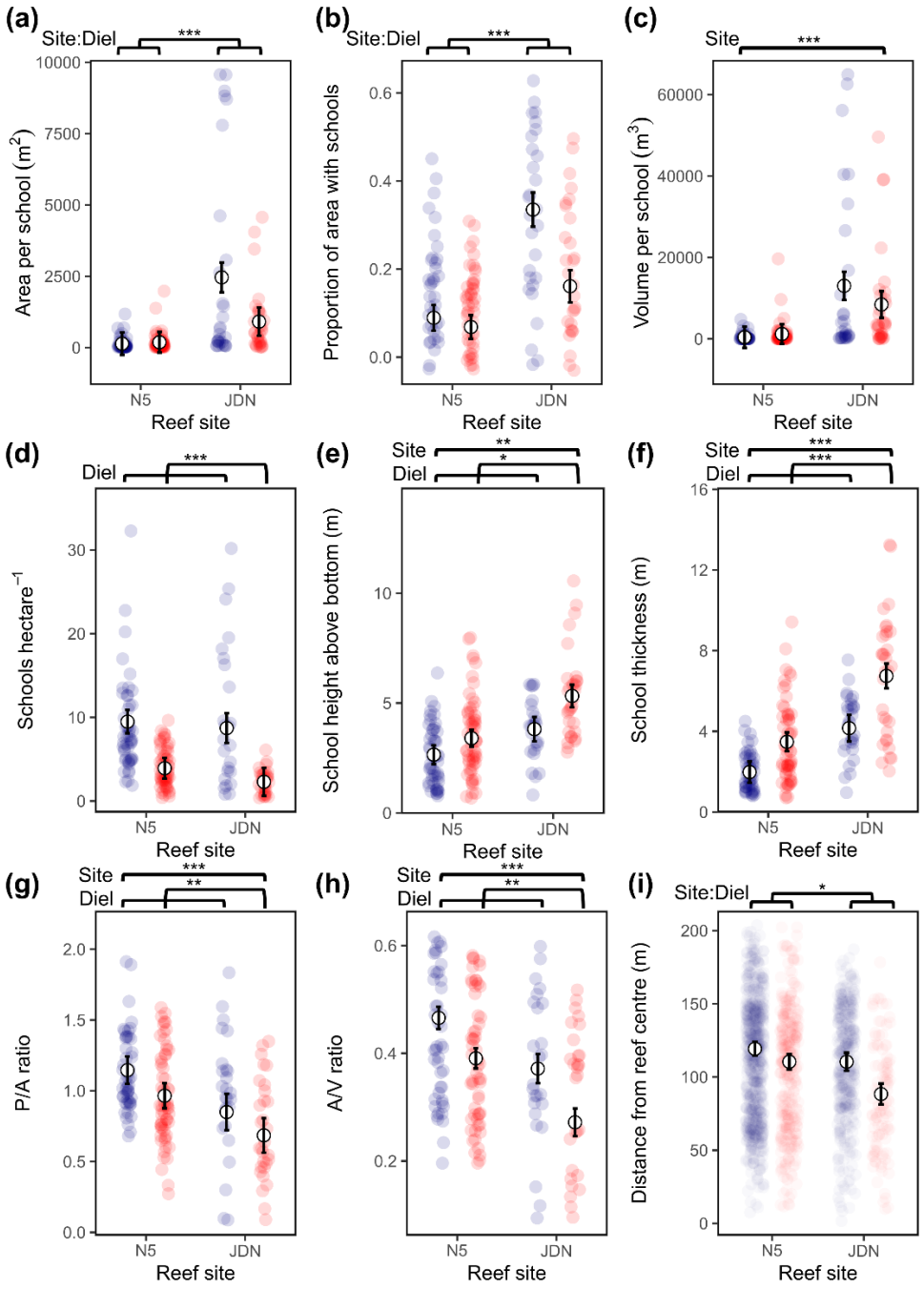

Figure 8 GLS model effects displaying mean values (symbols) and 95% confidence intervals for the interaction of reef site (N5 natural, JDN artificial) and diel period (night: blue and day: red) with variables describing school characteristics, including area of an individual school (a), proportion of surveyed area containing schools (b), volume of individual schools (c), number of schools per hectare of area surveyed (d), school height above the seafloor (e), school thickness, or the sum of each 1 m depth interval containing fish (f), perimeter to area ratio (g), area to volume ratio (h) and horizontal distance from the reef centre (i). Significant fixed effects (Site, Diel) or variable interactions (Site:Diel) are indicated above each panel, along with significance level (*: $p < 0.05$, **: $p < 0.01$, ***: $p < 0.001$). Raw data are included for each combination of factors. Note, all models also contain a fixed effect for survey date to account for day-to-day variability (not shown).

Supplementary material

Supplementary text

Text S1. Determining school distribution from acoustic data

These methods have been adapted from Holland et al. (2021). We used the bathymetry detection tool in Echoview, along with the known geographic locations of reef structures and their dimensions, to construct bathymetry surfaces which were inclusive of artificial structures. These updated bathymetry surfaces were used to subset midwater acoustic data so that echoes from reef structures and seafloor could be completely excluded. We then calculated median values across every three pings, blurred the data with an XYZ convolution, and applied a threshold of -65 dB to create a 3D Boolean mask to extract the original unaltered data. Georeferenced samples were exported from Echoview and all further analysis was conducted in R v3.6.3 (R Core Team 2020).

Georeferenced midwater samples were converted to 1 m resolution horizontal rasters using the 'rasterize' function from the 'raster' package (Hijmans 2020) in R. Three raster layers were created for each transect, to represent the minimum and maximum depth of target detections, as well as the 'school thickness' for each grid cell. We calculated school thickness by binning samples into vertical depth layers of 1 m, and for each horizontal grid cell, counting the number of layers containing at least one target detection. At 1 m resolution, this school thickness variable could essentially be considered aggregated school volume for each 1 m^2 of seafloor.

For transects undertaken to map school distribution, gridded values were aggregated to 5 m resolution by calculating mean values across cells, to improve computational efficiency (Figure 2). Transects from the same survey were combined into a single raster by calculating the mean value of overlapping cells. Raster extent was then cropped to a 200 m square grid

centred over each reef. Transect data for school characteristics retained the finer 1 m resolution so image analysis techniques could be used to define fine-scale school boundaries. Transects were processed individually, rather than being combined into single raster. These transects were subset to conform to a 300 m square grid.

Text S2. Identifying schools

For the study of diel effects on school characteristics, an image analysis process based on Reid and Simmonds (1993) was used to extract fish schools from gridded school thickness data. Initially a 'blur' filter, essentially a weighted mean function with a 3 × 3 kernel, was applied to each transect to remove background noise (Supplementary Figure 4) caused by zooplankton and isolated fish, using the following kernel weighting recommended in Reid and Simmonds (1993):

$$\begin{matrix} 1 & 2 & 1 \\ 2 & 1 & 2 \\ 1 & 2 & 1 \end{matrix}$$

This was followed by binary thresholding of the blurred data, using a threshold value selected by examining the frequency histogram of school thickness. In this case, 2 m was selected as the minimum school thickness threshold because it excluded the largest spike in frequency to result from noise. Approximately 50% of transects had a mean value above this threshold.

To further isolate schools we then applied an erosion filter to this binary data, which takes the minimum value of an unweighted 3 × 3 kernel. We subsequently applied a dilation, which takes the maximum value of an identical unweighted kernel. The erosion followed by dilation steps essentially remove a layer of pixels, and then add a layer of pixels back to each object, respectively (Reid & Simmonds 1993). This removes isolated nonzero pixels and smooths school edges, further cleaning the data and eliminating individual targets and returns not likely to be aggregations. Following this, objects in the binary data were converted to

polygons, which were used to extract the original unprocessed data. In this way, aggregations were defined and isolated so that statistics, such as perimeter and area, could be calculated for each aggregation.

Literature cited in supplementary

Hijmans RJ (2020) raster: Geographic Data Analysis and Modeling. R package version 3.3-13

Holland MM, Becker A, Smith JA, Everett JD, Suthers IM (2021) Characterizing the three-dimensional distribution of schooling reef fish with a portable multibeam echosounder. Limnology and Oceanography: Methods

R Core Team (2020) R: A language and environment for statistical computing. R Foundation for Statistical Computing, Vienna, Austria

Reid D, Simmonds E (1993) Image analysis techniques for the study of fish school structure from acoustic survey data. Canadian Journal of Fisheries and Aquatic Sciences 50:886-893

Smith JA, Cornwell WK, Lowry MB, Suthers IM (2017) Modelling the distribution of fish around an artificial reef. Marine and Freshwater Research 68:1955-1964

Supplementary tables

Table S1 Regression estimates for the three GLS models describing the total abundance, species richness and Shannon diversity of schooling fish around the artificial and natural reef sites. Select column names as follows: DF – total degrees of freedom, R DF – residual degrees of freedom, SE Mod – model standard error, ΔAIC date – ΔAIC with date as the only predictor, p – p-value from ANOVA of specified model and model with date as only predictor, Estimate – coefficient estimate, SE term – standard error of the specified term, Pr(>|t|) – p-value of the specified term. Significance level of Pr(>|z|) indicated by .: > 0.05, *: ≤ 0.05, **: ≤ 0.01, ***: ≤ 0.001, ****: ≤ 0.0001.

Response	DF	R DF	SE Mod	ΔAIC date	p		Predictor	Estimate	SE Term	t-value	Pr(>|t|)	
Total abundance	70	62	126.89	5.1	0.008	**	intercept	-30.49	45.58	-0.67	0.506	.
							reef JDN	82.77	32.23	2.57	0.013	*
							date 2019-09-03	228.90	60.30	3.80	< 0.001	***
							date 2019-09-26	37.30	60.30	0.62	0.539	.
							date 2019-10-31	59.40	60.30	0.99	0.328	.
							date 2019-11-08	-1.50	60.30	-0.02	0.980	.
							date 2020-08-18	69.40	60.30	1.15	0.254	.
							date 2020-08-28	37.90	60.30	0.63	0.532	.

Response	DF	R DF	SE Mod	ΔAIC date	p		Predictor	Estimate	SE Term	t-value	Pr(>|t|)	
Species richness	70	62	0.96	20.1	< 0.001	***	intercept	2.19	0.35	6.33	< 0.001	***
							reef JDN	-1.17	0.24	-4.80	< 0.001	***
							date 2019-09-03	0.00	0.46	0.00	1.000	.
							date 2019-09-26	-0.20	0.46	-0.44	0.663	.
							date 2019-10-31	0.40	0.46	0.88	0.385	.
							date 2019-11-08	-1.10	0.46	-2.41	0.019	*
							date 2020-08-18	0.50	0.46	1.09	0.278	.
							date 2020-08-28	-0.90	0.46	-1.97	0.053	.

Response	DF	R DF	SE Mod	ΔAIC date	p		Predictor	Estimate	SE Term	t-value	Pr(>|t|)	
Shannon diversity	70	62	0.26	20.4	< 0.001	***	intercept	0.59	0.09	6.31	< 0.001	***
							reef JDN	-0.32	0.07	-4.84	< 0.001	***
							date 2019-09-03	-0.25	0.12	-2.04	0.046	*
							date 2019-09-26	-0.24	0.12	-1.91	0.061	.
							date 2019-10-31	0.02	0.12	0.18	0.860	.
							date 2019-11-08	-0.36	0.12	-2.91	0.005	**
							date 2020-08-18	0.02	0.12	0.16	0.877	.
							date 2020-08-28	-0.35	0.12	-2.86	0.006	**

Table S2 Regression estimates for the eight GLS models describing the area per school, proportion of area with schools, volume per school, schools hectare^{-1}, P/A ratio, A/V ratio, school height above bottom and school thickness of schooling fish around the artificial and natural reef sites. Select column names as follows: DF – total degrees of freedom, R DF – residual degrees of freedom, SE Mod – model standard error, ΔAIC date – ΔAIC with date as the only predictor, p – p-value from ANOVA of specified model and model with date as only predictor, Estimate – coefficient estimate, SE term – standard error of the specified term, Pr(>|t|) – p-value of the specified term. Significance level of Pr(>|z|) indicated by .: > 0.05, *: ≤ 0.05, **: ≤ 0.01, ***: ≤ 0.001, ****: ≤ 0.0001.

Response	DF	R DF	SE Mod	ΔAIC date	p		Predictor	Estimate	SE Term	t-value	Pr(>|t|)	
Area per school	173	163	1372.5	48.1	< 0.001	***	intercept	-147.24	467.458	-0.31	0.753	.
							diel day	50.64	276.167	0.18	0.855	.
							reef site JDN	2325.96	329.554	7.06	< 0.001	***
							diel day : reef site JDN	-1603.16	451.645	-3.55	< 0.001	***
Proportion of area with schools	173	163	0.101	99.1	< 0.001	***	intercept	0.02	0.034	0.45	0.654	.
							diel day	-0.02	0.020	-1.03	0.307	.
							reef site JDN	0.25	0.024	10.09	< 0.001	***
							diel day : reef site JDN	-0.15	0.033	-4.60	< 0.001	***

Response	DF	R DF	SE Mod	ΔAIC date	p		Predictor	Estimate	SE Term	t-value	Pr(>|t|)	
Volume per school	173	163	9045.4	37.3	< 0.001	***	intercept	-2460.35	3080.904	-0.80	0.426	.
							diel day	788.76	1820.198	0.43	0.665	.
							reef site JDN	12627.20	2172.100	5.81	< 0.001	***
							diel day : reef site JDN	-5392.60	2976.727	-1.81	0.072	.
Schools hectare-1	173	163	4.6	48.2	< 0.001	***	intercept	8.37	1.577	5.31	< 0.001	***
							diel day	-5.56	0.954	-5.83	< 0.001	***
							reef site JDN	-0.77	1.136	-0.68	0.498	.
							diel day : reef site JDN	-0.86	1.540	-0.56	0.579	.
School height above bottom (m)	173	163	1.7	109.9	< 0.001	***	intercept	2.98	0.490	6.09	< 0.001	***
							diel day	0.75	0.295	2.54	0.012	*
							reef site JDN	1.16	0.351	3.30	0.001	**
							diel day : reef site JDN	0.76	0.477	1.60	0.112	.

Response	DF	R DF	SE Mod	ΔAIC date	p		Predictor	Estimate	SE Term	t-value	Pr(>|t|)	
School thickness (m)	173	163	1.67	93.4	< 0.001	***	intercept	0.50	0.592	0.84	0.402	.
							diel day	1.50	0.358	4.19	< 0.001	***
							reef site JDN	2.18	0.424	5.14	< 0.001	***
							diel day : reef site JDN	1.08	0.573	1.89	0.060	.
P/A ratio	173	163	0.34	29.4	< 0.001	***	intercept	1.17	0.114	10.22	< 0.001	***
							diel day	-0.18	0.068	-2.68	0.008	**
							reef site JDN	-0.30	0.081	-3.68	< 0.001	***
							diel day : reef site JDN	0.02	0.110	0.15	0.883	.
A/V ratio	173	163	0.07	98.7	< 0.001	***	intercept	0.47	0.024	19.59	< 0.001	***
							diel day	-0.08	0.014	-5.25	< 0.001	***
							reef site JDN	-0.09	0.017	-5.51	< 0.001	***
							diel day : reef site JDN	-0.02	0.023	-1.05	0.294	.

Response	DF	R DF	SE Mod	ΔAIC date	p		Predictor	Estimate	SE Term	t-value	Pr(>|t|)	
Distance from reef centre (m)	1464	1454	29.1	44.8	< 0.001	***	intercept	113.33	6.92	16.38	< 0.001	***
							diel day	-8.82	3.53	-2.50	0.012	*
							reef site JDN	-8.83	3.90	-2.26	0.024	*
							diel day : reef site JDN	-13.23	5.88	-2.25	0.025	*

Supplementary figures

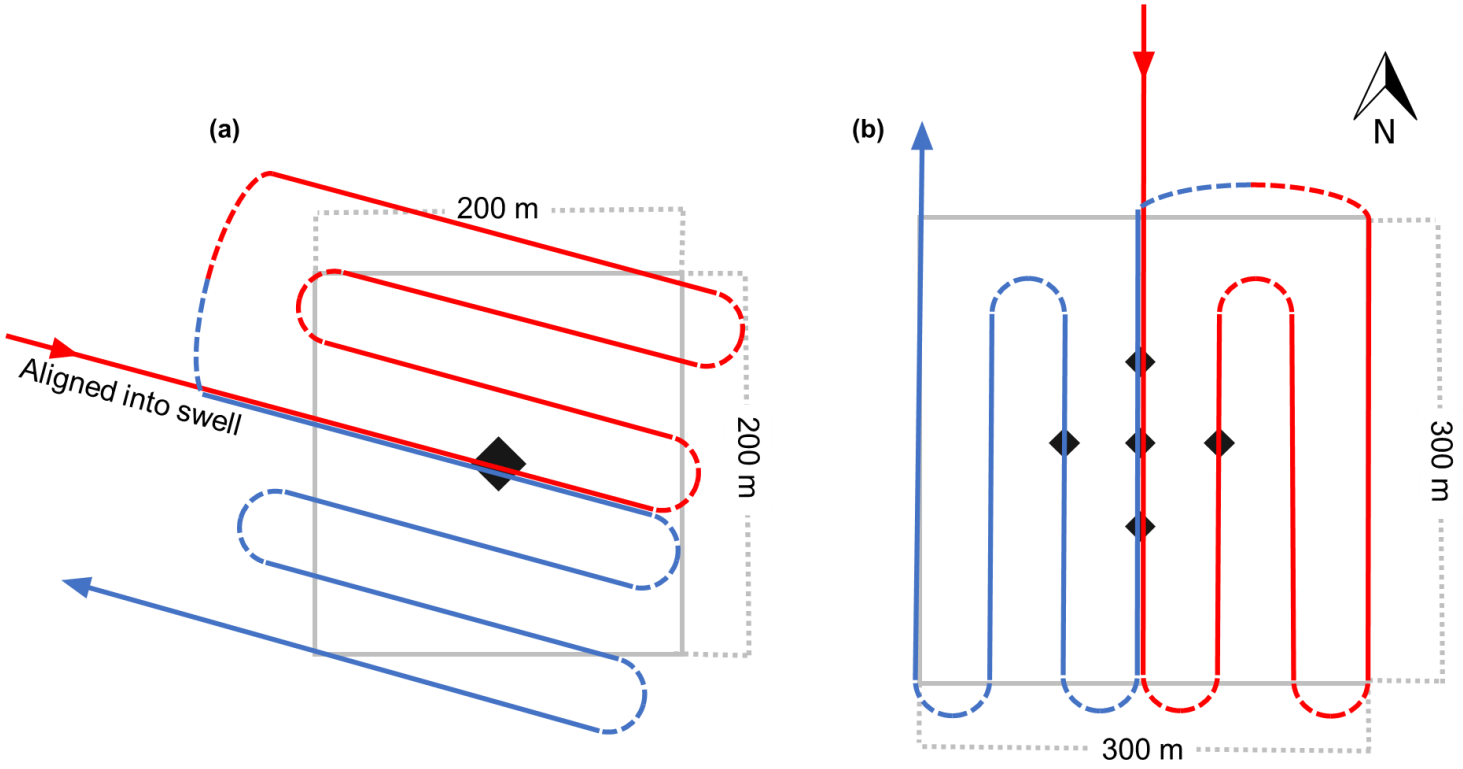

Figure S1 Transect patterns for surveying school distribution (a) and diel effects on school characteristics (b), with (a) aligned into the prevailing swell and (b) along lines of constant longitude, starting with red arrow, and ending with the blue arrow. Red lines represent the first set of transects and blue lines represent the second set of transects. Dashed lines indicate sections of the vessel track which were excluded from analysis. The black diamonds indicate the reef centre, or the reef structures in the case of artificial reefs. All data outside grey boxes were excluded from analyses.

Figure S2 A schematic diagram of the camera assembly used for drifting and benthic remote video deployments (from Smith et al. 2017).

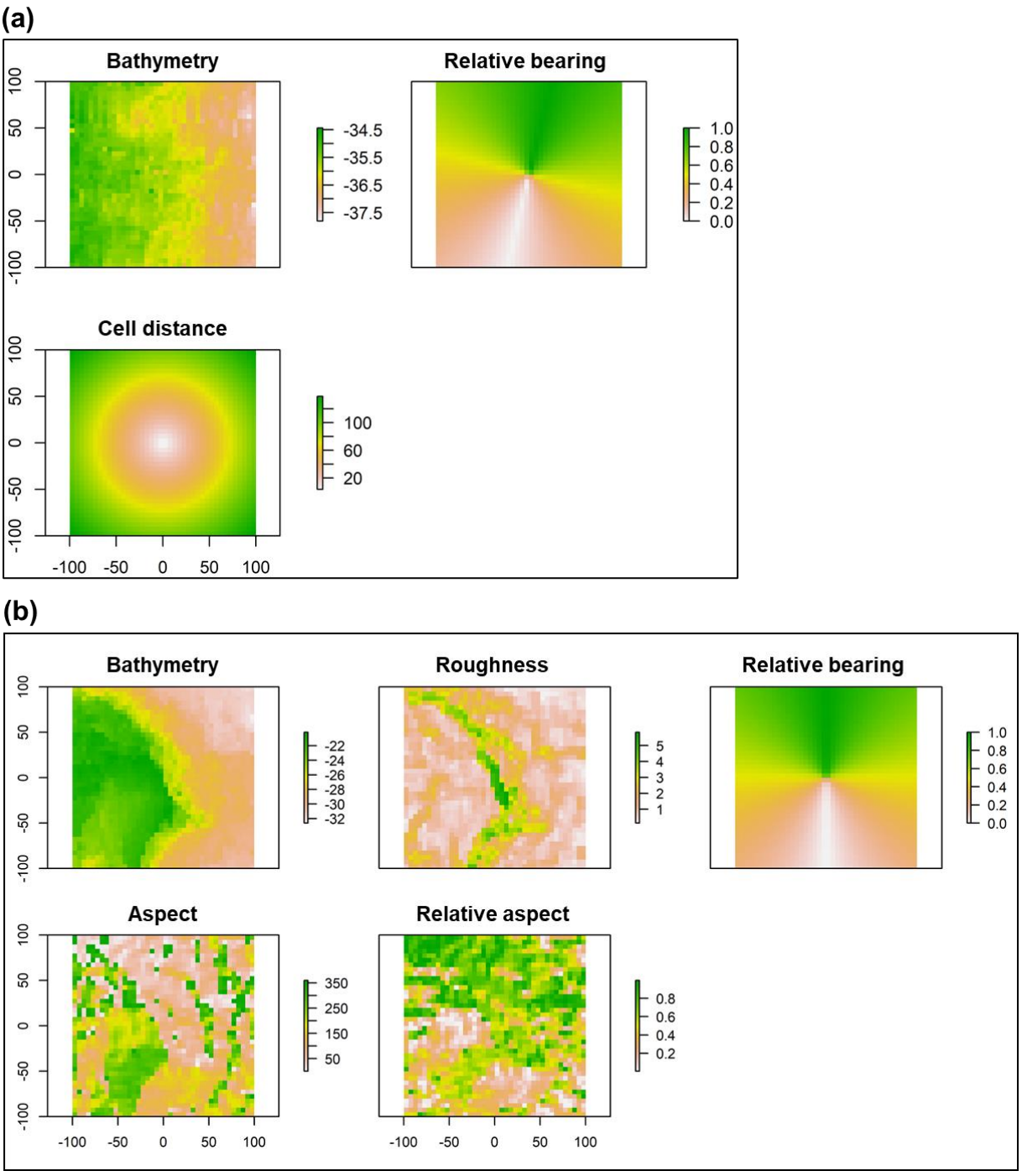

Figure S3 Examples of raster surfaces used to generate explanatory variables on a per-survey basis for the artificial reefs (a) and the natural reef (b) models. The examples provided are from site OAR (a) and N1 (b).

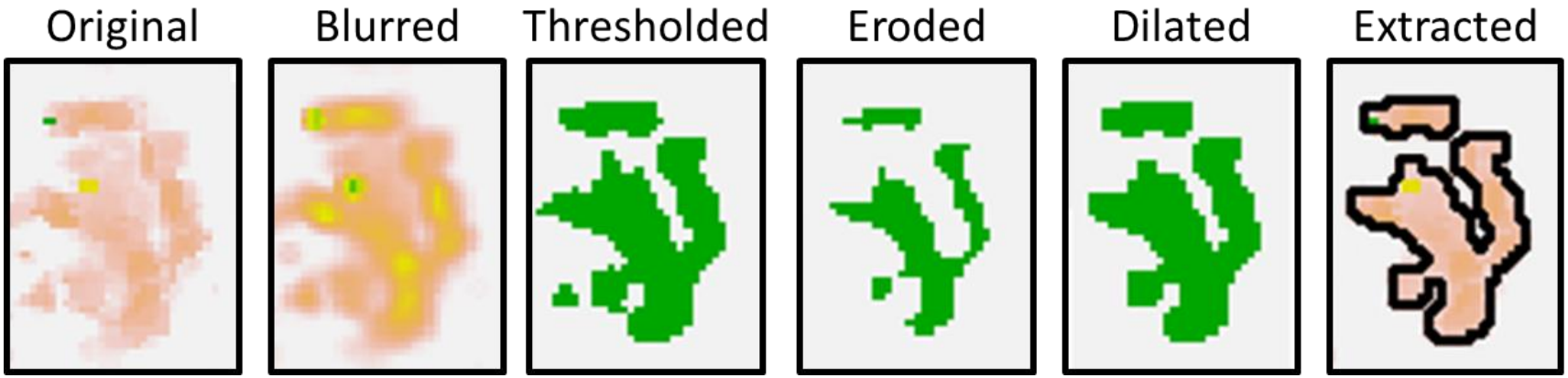

Figure S4 An illustrated example of the six-step image analysis process for isolating fish schools from rasterised multibeam echosounder data. Pixel size is 1 m.

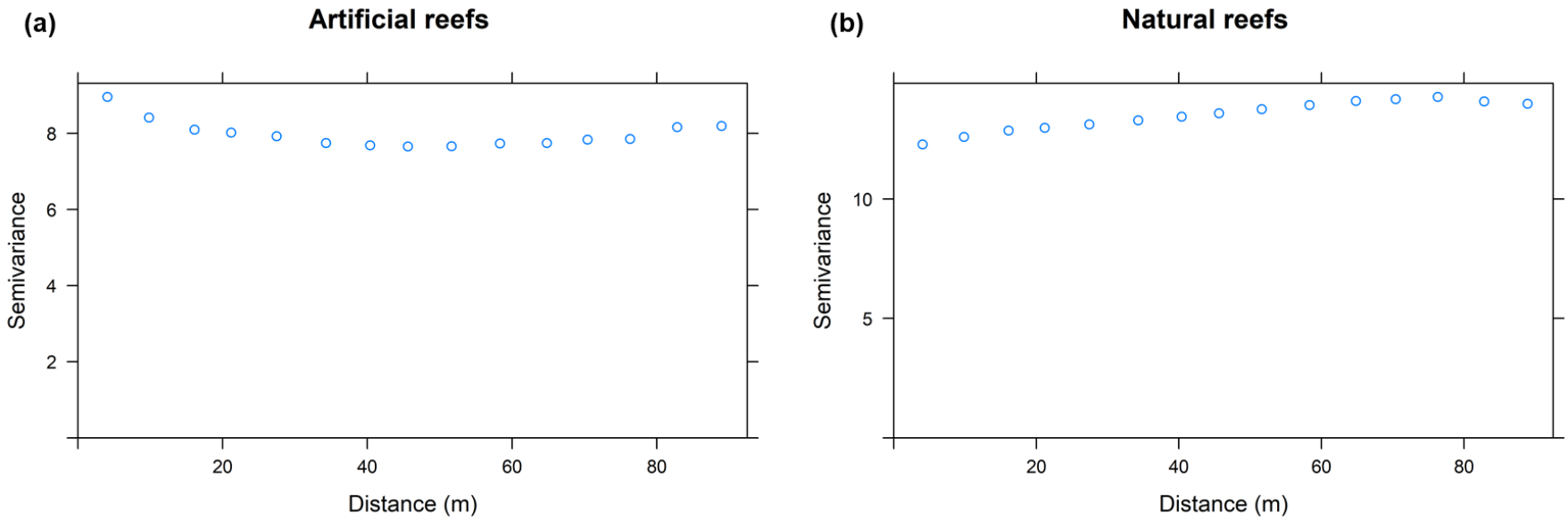

Figure S5 Semivariograms generated from spatially referenced residuals for the final artificial reef (a) and natural reef (b) models.

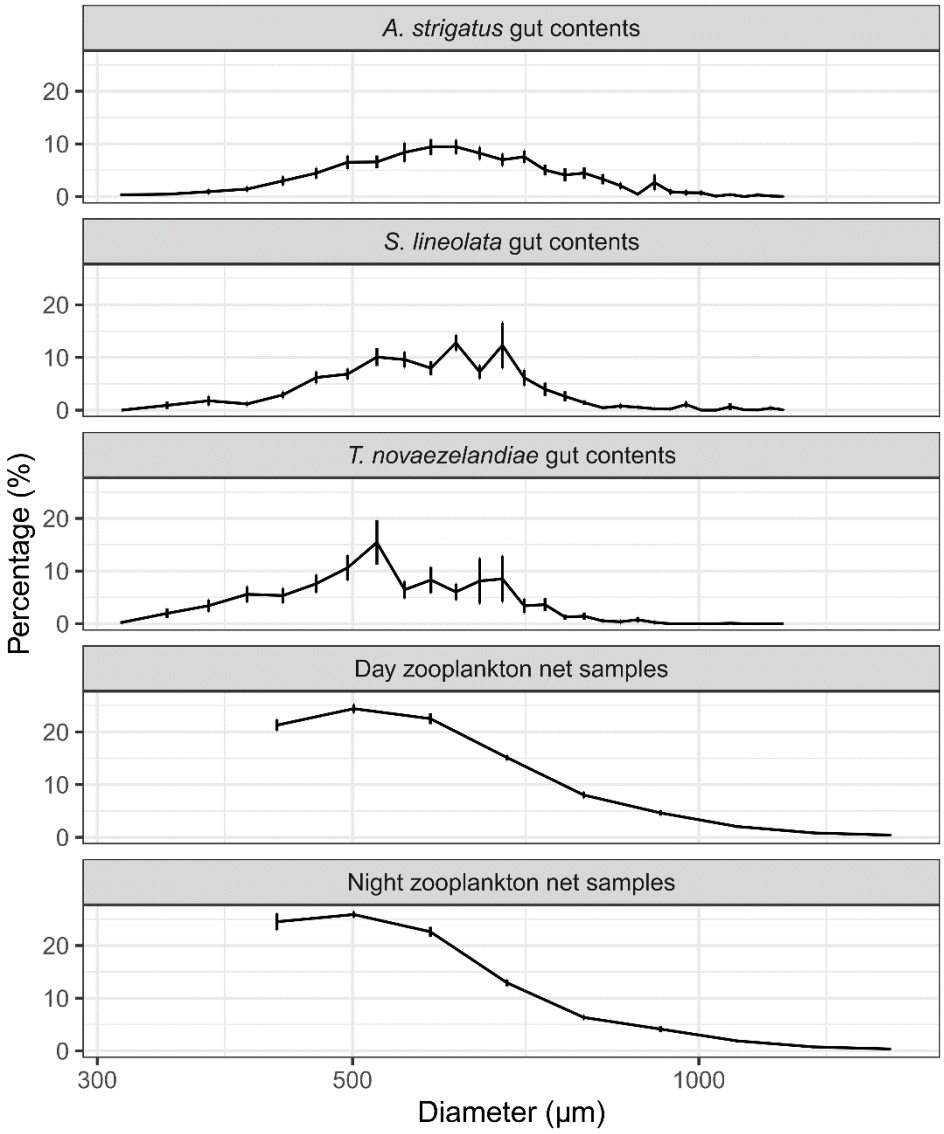

Figure S6 Comparison of the average prey (from gut contents analysis of three fish species, Schilling et al. unpublished data) and day/night zooplankton net capture size distributions. Error bars represent standard error of the mean.